COMMUNICATIONS IN COMPUTATIONAL PHYSICS
Vol. **2**, No. 1, pp. 1-53

Commun. Comput. Phys.
February 2007

Recent Progress in Symplectic Algorithms for Use in Quantum Systems

Xue-Shen Liu[1,*], Yue-Ying Qi[1,2], Jian-Feng He[1,3] and Pei-Zhu Ding[1]

[1] *Institute of Atomic and Molecular Physics, Jilin University, Changchun 130012, P. R. China.*
[2] *School of Electrical Engineering, Jiaxing University, Jiaxing 314001, P. R. China.*
[3] *Department of Physics, School of Science, Beijing Institute of Technology, Beijing 100081, P. R. China.*

Received 20 December 2005; Accepted (in revised version) 5 April 2006

Available online 30 August 2006

Abstract. In this paper we survey recent progress in symplectic algorithms for use in quantum systems in the following topics: Symplectic schemes for solving Hamiltonian systems; Classical trajectories of diatomic systems, model molecule A_2B, Hydrogen ion H_2^+ and elementary atmospheric reaction $N(^4S)+O_2(X^3\Sigma_g^-)\rightarrow NO(X^2\Pi)+O(^3P)$ calculated by means of Runge-Kutta methods and symplectic methods; the classical dissociation of the HF molecule and classical dynamics of H_2^+ in an intense laser field; the symplectic form and symplectic-scheme shooting method for the time-independent Schrödinger equation; the computation of continuum eigenfunction of the Schrödinger equation; asymptotic boundary conditions for solving the time-dependent Schrödinger equation of an atom in an intense laser field; symplectic discretization based on asymptotic boundary condition and the numerical eigenfunction expansion; and applications in computing multi-photon ionization, above-threshold ionization, Rabbi oscillation and high-order harmonic generation of laser-atom interaction.

PACS: 47.10.Df, 02.70.-c, 34, 95.30.-k

Key words: Quantum system, symplectic algorithm, classical trajectory, Schrödinger equation, intense laser field.

Contents

*Corresponding author. *Email addresses:* liuxs@jlu.edu.cn (X. S. Liu), jess1234yao@yahoo.com.cn (Y. Y. Qi), hjf@bit.edu.cn (J. F. He), dpz@mail.jlu.edu.cn (P. Z. Ding)

 ©2007 Global-Science Press

DOI https://doi.org/2007-CiCP-7894 | Generated on 2024-12-22 17:59:56
OPEN ACCESS

1 Introduction

The fundamental theorem of Hamiltonian mechanics says that the time-evolution of a Hamiltonian system is the evolution of symplectic transformation. In this sense, we say that the Hamiltonian system has a symplectic structure [1, 2]. Therefore, Ruth [3] and Feng [4] presented the symplectic algorithm for solving the Hamiltonian system, which leads to a new method for solving the Hamiltonian mechanics. It is now well known that the symplectic algorithm is a difference method that preserves the symplectic structure, and it is the method of choice in the long-time calculation and for preserving the structure of the system [5, 7].

At present, the study and application of symplectic algorithms is well developed [4]-[27]. In particular, Feng [6] constructed symplectic difference schemes of Hamiltonian formalism via generating functions, and higher order symplectic schemes and multi-stage symplectic schemes were presented in [7, 8, 86]. Moreover, symplectic partitioned Runge-Kutta methods were deduced [12, 22], and multi-symplectic schemes were also established [24–27]. Up to now, symplectic methods have been applied to many fields, for example, to the nonlinear Schrödinger equation [28–32], celestial mechanics equation [33–35], time-evolution of quantum systems [36–39], molecular dynamics [40, 41], plasma physics [42], the KdV equation, the evolution of vortices in a rotating Bose–Einstein Condensate, and so on.

A quantum system is an infinite-dimensional Hamiltonian system. The time-evolution of the time-dependent Schrödinger equation preserves the normalization and symplectic product of the wave function. Thus, the time-dependent Schrödinger equation can be transformed into a Hamiltonian canonical equation. The square-preserving and symplectic scheme is the reasonable and natural way for solving the time-dependent Schrödinger equation. Therefore, the symplectic algorithm of the classical Hamiltonian system was extended to the time-evolution of quantum system [43, 44].

In this paper, we will review the applications of the symplectic algorithm of the classical Hamiltonian system to the quantum system. The topics of this review article include

a. Symplectic space, explicit symplectic schemes for linear separate Hamiltonian systems and tailored to the time-dependent Hamiltonian function;
b. The classical theory and classical trajectory methods and the classical dynamics of molecular system in an intense laser field;

DOI https://doi.org/2007-CiCP-7894 | Generated on 2024-12-22 17:59:56
OPEN ACCESS

c. The time-independent Schrödinger equation and symplectic-scheme shooting method; the computation of the continuum eigenfunction of the one-dimensional time-independent Schrödinger equation;
d. The interaction of an atom with an intense laser field and the asymptotic boundary conditions for solving the time-dependent Schrödinger equation of atom in an intense laser field, symplectic discretizations based on the asymptotic boundary condition and the numerical eigenfunction expansion and applications in computing multi-photon ionization, above-threshold ionization, Rabbi oscillation and high-order harmonic generation of laser-atom interaction.

2 Hamiltonian systems and symplectic algorithms

We first introduce the fundamental theorem of Hamiltonian mechanics, and then give some symplectic schemes for solving Hamiltonian systems.

2.1 Legendre transformation of classical mechanics

The classical mechanics tells us that the motion of a mechanics $\vec{r}(t)=(x_1(t),\cdots x_n(t))$, for example the motion of mass system in the potential field $U(\vec{r})$, is depicted by the Newtonian equation

$$\frac{d}{dt}(m_i\dot{x}_i)+\frac{\partial U}{\partial x_i}=0,\quad (i=1,\cdots,n), \tag{2.1}$$

where $\dot{x}_i:=dx_i/dt$. The system of equation (2.1) is equipped with the $2n$ initial conditions: $x_i(t_0)=x_i^0,\dot{x}_i(t_0)=\dot{x}_i^0$, $(i=1,\cdots,n)$.

2.1.1 Hamiltonian principle of least action

Theorem 2.1 ([2]). *Suppose $L=T-U$, where $T=\frac{1}{2}\sum_i m_i\dot{x}_i^2$ and $U=U(\vec{r})$ are the kinetic and potential energy of the mechanical system* (2.1)*, respectively. Then the motion $\vec{r}(t)$ of the mechanics system* (2.1) *coincides with the extremals of the functional*

$$\Phi(\vec{r})=\int_{t_0}^{t_1}L(\vec{r},\dot{\vec{r}},t)dt. \tag{2.2}$$

Contrarily, the extremals of the functional (2.2) *coincide with the motion of the mechanics system* (2.1).

Definition 2.1 ([2]). Given a mechanics system. Let $\vec{q}=(q_1,\cdots,q_n)$ be the generalized coordinate and $\dot{\vec{q}}=(\dot{q}_1,\cdots,\dot{q}_n)$ the generalized velocity. We call

$$L(\vec{q},\dot{\vec{q}},t)=T-U=\frac{1}{2}\sum_i m_i\dot{q}_i^2-U(q_1,q_2,\cdots,q_n) \tag{2.3}$$

the Lagrangian function of the mechanics system.

DOI https://doi.org/2007-CiCP-7894 | Generated on 2024-12-22 17:59:56
OPEN ACCESS

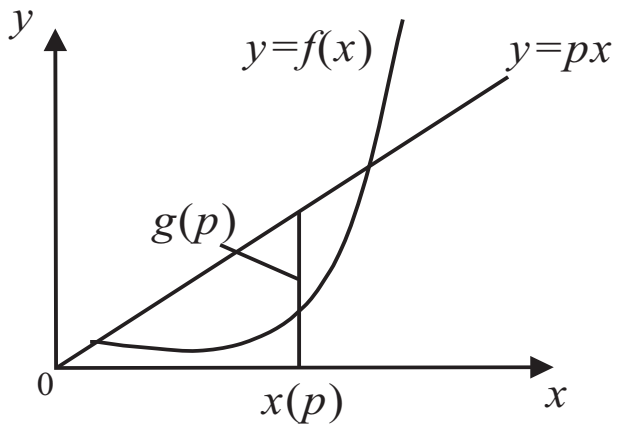

Figure 1: Legendre transformation.

Some more definitions are given below: $\partial L/\partial q_i$ is called the generalized mechanics, $p_i := \partial L/\partial \dot{q}_i$ is called the generalized momentum, the functional $\Phi(\vec{r}) = \int_{t_0}^{t_1} L(\vec{r},\dot{\vec{r}},t)dt$ is called the action, and the equation

$$\frac{d}{dt}\left(\frac{\partial L}{\partial \dot{q}_i}\right) - \frac{\partial L}{\partial q_i} = 0, \quad (i=1,\cdots,n) \tag{2.4}$$

is called the Lagrangian equation. Theorem 2.1 illustrates that the Newtonian equation (2.1) and the Lagrangian equation (2.4) are equivalent, both of them depict the motion of the mechanics system.

2.1.2 Legendre transformation of classical mechanics

Let $y = f(x)$ be a convex function, $f''(x) > 0$. We draw a graph of $y = f(x)$ in the (x,y) plane, see Fig. 1. Let p be a given real number. Consider the straight line $y = px$, and denote $F(p,x) = px - f(x)$, which is the difference between the line $y = px$ and the curve $y = f(x)$. Due to $f''(x) > 0$, $F(p,x)$ has a maximum with respect to x at the unique point $x(p)$; the point $x(p)$ can be found by the condition $\partial F/\partial x = 0$, i.e., $f'(x) = p$. For every value of p, $F(p,x) = px - f(x)$ has a maximum at the unique point $x(p)$.

Now we define $g(p) = F(p,x(p))$, where $g(p)$ is called the Legendre transformation of the function $f(x)$. We can see from Fig. 1 that $g(p)$ is the maximum of $F(p,x) = px - f(x)$ at the point p, i.e.,

$$g(p) = \max_x F(p,x).$$

2.1.3 Legendre transformation for many variables

Let $f(\vec{x}) = f(x_1,\cdots,x_n)$ be a convex function of n variables $\vec{x} = (x_1,\cdots,x_n)$, so that $(\frac{\partial^2 f}{\partial \vec{x}^2} d\vec{x}, d\vec{x})$ is a positive definite quadratic form. Let $\vec{p} = (p_1,\cdots,p_n)$ be an n-dimensional real

DOI https://doi.org/2007-CiCP-7894 | Generated on 2024-12-22 17:59:56
OPEN ACCESS

vector and $F(\vec{p},\vec{x})=(\vec{p},\vec{x})-f(\vec{x})$ be a real function. Then

$$g(\vec{p})=F(\vec{p},x(\vec{p}))=\max_{\vec{x}}F(\vec{p},\vec{x})$$

is called the *Legendre transformation* of $f(\vec{x})$, where $\vec{x}(\vec{p})$ can be defined by the condition $\partial f/\partial\vec{x}=\vec{p}$.

2.2 Classical Hamiltonian system and symplectic space

The materials of this subsection can be found in [1–6]. By means of a Legendre transformation, a Lagrangian system of a second-order differential equation can be converted into a symmetrical system of $2n$ first-order equation which is called the Hamiltonian canonical equation.

2.2.1 Classical Hamiltonian system

The Lagrangian equation (2.4) can be written in vector form,

$$\frac{d}{dt}\left(\frac{\partial L}{\partial\dot{\vec{q}}}\right)-\frac{\partial L}{\partial\vec{q}}=0. \tag{2.5}$$

We know that the generalized momentum is $\vec{p}=\partial L/\partial\dot{\vec{q}}$, and thus we have $\dot{\vec{p}}=\partial L/\partial\vec{q}$. Suppose that Lagrangian function is $L(\vec{q},\dot{\vec{q}},t)$: $\mathbb{R}^n\times\mathbb{R}^n\times\mathbb{R}\to\mathbb{R}$, which is convex with respect to the second variables $\dot{\vec{q}}$, $\partial^2L/\partial\dot{q}_i^2>0, i=1,\cdots,n$.

Theorem 2.2. *The system of Lagrangian equations* (2.5) *is equivalent to the system of* $2n$ *first-order Hamiltonian equations,*

$$\dot{\vec{p}}=-\frac{\partial H}{\partial\vec{q}},\quad \dot{\vec{q}}=\frac{\partial H}{\partial\vec{p}}, \tag{2.6}$$

or equivalently,

$$\dot{p}_i=-\frac{\partial H}{\partial q_i},\quad \dot{q}_i=\frac{\partial H}{\partial p_i},\quad (i=1,\cdots,n), \tag{2.7}$$

where the Hamiltonian function $H(\vec{p},\vec{q},t)$ *is the Legendre transform of the Lagrangian function* $L(\vec{q},\dot{\vec{q}},t)$ *viewed as a function of* $\dot{\vec{q}}$*, i.e.,*

$$H(\vec{p},\vec{q},t)=\max_{\dot{\vec{q}}}\left\{\vec{p}\dot{\vec{q}}-L(\vec{q},\dot{\vec{q}},t)\right\}. \tag{2.8}$$

2.2.2 Symplectic space

`Symplectic space.` Let $\mathbb{R}^{2n}$ be the $2n$-dimensional real linear space, and $x=(x_1,\cdots,x_{2n})^T$, with $x_j\in\mathbb{R}$, be a vector of $\mathbb{R}^{2n}$. Let

$$J=\begin{pmatrix}0 & I\\ -I & 0\end{pmatrix} \tag{2.9}$$

DOI https://doi.org/2007-CiCP-7894 | Generated on 2024-12-22 17:59:56
OPEN ACCESS

which is the standard symplectic matrix, where I is the $n\times n$ identical matrix. For $x\in\mathbb{R}^{2n}$ and $y\in\mathbb{R}^{2n}$, we define the symplectic product

$$[x,y]=\sum_{i=1}^{n}(x_iy_{n+i}-x_{n+i}y_i)=(x_1\cdots x_{2n})J\begin{pmatrix}y_1\\ \vdots\\ y_{2n}\end{pmatrix},$$

which is a bilinear anti-symmetric form. The space $\{\mathbb{R}^{2n},[x,y]\}$ is called the *symplectic space*. If we let $z=(p,q)^T$, the Hamiltonian equation (2.7) can be written as

$$\dot{z}=J^{-1}\frac{\partial H}{\partial z}. \tag{2.10}$$

Symplectic mapping. Let $\hat{S}:\mathbb{R}^{2n}\to\mathbb{R}^{2n}$ be a mapping. If $\hat{S}$ preserves the symplectic product, i.e.,

$$\left[\hat{S}(x),\hat{S}(y)\right]=[x,y],\quad x,y\in\mathbb{R}^{2n}, \tag{2.11}$$

then $\hat{S}$ is called the symplectic transformation or symplectic mapping. Moreover, if $\hat{S}$ is a linear transformation, and if we choose a basis vector in $\mathbb{R}^{2n}$, then $\hat{S}$ coincides with a matrix S, i.e.,

$$\hat{S}(e_1\cdots e_{2n})=(e_1\cdots e_{2n})S,\quad \hat{S}(x)=Sx, \tag{2.12}$$

where $x=(x_1,\cdots,x_{2n})^T=x_1e_1+\cdots+x_{2n}e_{2n}\in\mathbb{R}^{2n}$.

Theorem 2.3. *The linear transformation S is a symplectic transformation if and only if*

$$S^TJS=J. \tag{2.13}$$

We now give the definitions for *symplectic matrix* and *infinitesimal symplectic matrix*.

Definition 2.2. If the $2n$-order matrix S satisfies

$$S^TJS=J, \tag{2.14}$$

then S is called a symplectic matrix. If the $2n$-order matrix B satisfies

$$JB+B^TJ=0, \tag{2.15}$$

then B is called an infinitesimal symplectic matrix.

Theorem 2.4. *If the $2n$-order matrix A is an infinitesimal symplectic matrix, then its exponential transformation $\exp(A)$ is a symplectic matrix. If the $2n$-order matrix B is a symplectic matrix and $|I+B|\neq 0$, then*

$$F=(I+B)^{-1}(I-B) \tag{2.16}$$

is a symplectic matrix. F defined above is called the Cayley transformation of B.

DOI https://doi.org/2007-CiCP-7894 | Generated on 2024-12-22 17:59:56
OPEN ACCESS

The fundamental theorem of Hamiltonian mechanics. It is easy to verify that all $2n\times 2n$-order symplectic matrices form a group under matrix multiplication, which is called the *symplectic group* and denoted by $S_p(2n)$.

Theorem 2.5. *If S is a symplectic transformation,*

$$z=S(\hat{z}),\quad H(z)=H(S(\hat{z}))=\hat{H}(\hat{z}), \tag{2.17}$$

then the canonical equation (2.10) *can be transformed into*

$$\dot{\hat{z}}=J^{-1}\frac{\partial \hat{H}}{\partial \hat{z}}=J^{-1}\hat{H}_{\hat{z}}. \tag{2.18}$$

Theorem 2.6. *The solution of the canonical equation* (2.10) *is generated by a one-parameter symplectic group $\{g_H^t;-\delta<t<\delta\}$. That is to say, g_H^t is a symplectic transformation, g_H^0 is the identical transformation, $g_H^{t_1+t_2}=g_H^{t_1}\cdot g_H^{t_2}$. If $z(0)$ is the initial condition, then the solution of the canonical equation* (2.10) *is*

$$z(t)=g_H^t(z(0)). \tag{2.19}$$

g_H^t is called the phase flow of the canonical equation (2.10).

2.3 Symplectic algorithm

Based upon the fundamental theorem of Hamiltonian mechanics, Ruth [3] and Feng [4–6] presented the symplectic algorithm for solving the Hamiltonian system, and found a new method for solving the Hamiltonian mechanics. In this section, we will briefly describe the symplectic schemes for solving the Hamiltonian equation, and give some symplectic schemes often used in computational quantum systems.

2.3.1 Explicit symplectic scheme for linear separate Hamiltonian system

If we take the Hamiltonian function to be of a quadratic form

$$H(z)=\frac{1}{2}z^TGz,\qquad G^T=G, \tag{2.20}$$

then this Hamiltonian system is a linear system which can be written as

$$\frac{dz}{dt}=Bz,\quad B=J^{-1}G, \tag{2.21}$$

where G is a symmetric non-singular constant matrix. It is easy to verify that the matrix B is an infinitesimal symplectic matrix. The solution of the canonical equation (2.21) is

$$z(t)=g^t(z(0)),\quad g^t=\exp(tB).$$

The phase flow of the exponential transformation of an infinitesimal symplectic matrix is a symplectic matrix.

DOI https://doi.org/2007-CiCP-7894 | Generated on 2024-12-22 17:59:56
OPEN ACCESS

If the Hamiltonian system is separable, then the Hamiltonian function has the form

$$H(z)=H(p,q)=H_1(p)+H_2(q), \tag{2.22}$$

and the canonical equation is

$$\frac{dp}{dt}=-\frac{\partial H_2(q)}{\partial q}, \qquad \frac{dq}{dt}=\frac{\partial H_1(p)}{\partial p}. \tag{2.23}$$

If the Hamiltonian system is linear and separable, then the Hamiltonian function has the form

$$H(p,q)=\frac{1}{2}\left(p^T,q^T\right)G\begin{pmatrix} p \\ q \end{pmatrix}=\frac{1}{2}(p^TUp+q^TVq) \tag{2.24}$$
$$=\text{kinetic energy} + \text{potential energy},$$

where

$$G=\begin{pmatrix} U & 0 \\ 0 & V \end{pmatrix},$$

U is symmetric positive definite and $V=V^T$. Then the canonical equation becomes

$$\frac{dp}{dt}=-Vq, \qquad \frac{dq}{dt}=Up. \tag{2.25}$$

Now we give explicit symplectic schemes for solving a separable Hamiltonian system. Let τ be the time step, and $z^n=z(n\tau)$, $n=1,2,\cdots$.

Scheme I. For the Hamiltonian system (2.20), the Euler-centered scheme

$$\frac{1}{\tau}(z^{n+1}-z^n)=B\frac{1}{2}\cdot(z^{n+1}+z^n) \tag{2.26}$$

is a 2nd-order symplectic scheme, which gives the transformation from z^n to z^{n+1},

$$z^{n+1}=F_\tau z^n, \quad F_\tau=\left(I-\frac{\tau}{2}B\right)^{-1}\left(I+\frac{\tau}{2}B\right)=\psi\left(-\frac{\tau}{2}B\right), \tag{2.27}$$

where $\psi(\lambda)=(1-\lambda)/(1+\lambda)$, $\psi(B)$ is the Cayley transformation of matrix B. It is easy to verify that $\psi(B)$ is a symplectic matrix if B is an infinitesimal symplectic matrix.

For linear and separable Hamiltonian system (2.24), the symplectic scheme (2.26) becomes

$$\frac{1}{\tau}(p^{n+1}-p^n)=-V\frac{1}{2}\cdot(q^{n+1}+q^n), \quad \frac{1}{\tau}(q^{n+1}-q^n)=U\frac{1}{2}\cdot(p^{n+1}+p^n). \tag{2.28}$$

Scheme II. For the linear and separable Hamiltonian system (2.24), the scheme

$$\frac{1}{\tau}(p^{n+1}-p^n)=-Vq^{n+\frac{1}{2}}, \quad \frac{1}{\tau}(q^{n+\frac{1}{2}+1}-q^{n+\frac{1}{2}})=Up^{n+1} \tag{2.29}$$

is a 2nd-order explicit symplectic scheme.

For a separable Hamiltonian system (2.22), explicit symplectic schemes are often used. These include

DOI https://doi.org/2007-CiCP-7894 | Generated on 2024-12-22 17:59:56
OPEN ACCESS

- The 1st-order explicit symplectic scheme:

$$p^{n+1}=p^n-\tau\left(\frac{\partial H_2}{\partial q}\right)_{q^n},\qquad q^{n+1}=q^n+\tau\left(\frac{\partial H_1}{\partial p}\right)_{p^{n+1}};\tag{2.30}$$

- The 2-stage, 2nd-order explicit symplectic scheme:

$$\begin{aligned}&p_1=p^n,&&q_1=q^n+\frac{\tau}{2}\left(\frac{\partial H_1}{\partial p}\right)_{p_1},\\&p^{n+1}=p_1-\tau\left(\frac{\partial H_2}{\partial q}\right)_{q_1},&&q^{n+1}=q_1+\frac{\tau}{2}\left(\frac{\partial H_1}{\partial p}\right)_{p^{n+1}};\end{aligned}\tag{2.31}$$

- The 3-stage, 3rd-order explicit symplectic scheme:

$$\begin{aligned}&p_1=p^n-c_1\tau\left(\frac{\partial H_2}{\partial q}\right)_{q^n},&&q_1=q^n+d_1\tau\left(\frac{\partial H_1}{\partial p}\right)_{p_1},\\&p_2=p_1-c_2\tau\left(\frac{\partial H_2}{\partial q}\right)_{q_1},&&q_2=q_1+d_2\tau\left(\frac{\partial H_1}{\partial p}\right)_{p_2},\\&p^{n+1}=p_2-c_3\tau\left(\frac{\partial H_2}{\partial q}\right)_{q_2},&&q^{n+1}=q_2+d_3\tau\left(\frac{\partial H_1}{\partial p}\right)_{p^{n+1}},\end{aligned}\tag{2.32}$$

where

$$c_1=\frac{7}{24},\ c_2=\frac{3}{4},\ c_3=-\frac{1}{24},\ d_1=\frac{2}{3},\ d_2=-\frac{2}{3},\ d_3=1,\tag{2.33}$$

or

$$c_1=1,\ c_2=-\frac{2}{3},\ c_3=\frac{2}{3},\ d_1=-\frac{1}{24},\ d_2=\frac{3}{4},\ d_3=\frac{7}{24};\tag{2.34}$$

- The 4-stage, 4th-order explicit symplectic scheme:

$$\begin{aligned}&p_1=p^n-c_1\tau\left(\frac{\partial H_2}{\partial q}\right)_{q^n},&&q_1=q^n+d_1\tau\left(\frac{\partial H_1}{\partial p}\right)_{p_1},\\&p_2=p_1-c_2\tau\left(\frac{\partial H_2}{\partial q}\right)_{q_1},&&q_2=q_1+d_2\tau\left(\frac{\partial H_1}{\partial p}\right)_{p_2},\\&p_3=p_2-c_3\tau\left(\frac{\partial H_2}{\partial q}\right)_{q_2},&&q_3=q_2+d_3\tau\left(\frac{\partial H_1}{\partial p}\right)_{p_3},\\&p^{n+1}=p_3-c_4\tau\left(\frac{\partial H_2}{\partial q}\right)_{q_3},&&q^{n+1}=q_3+d_4\tau\left(\frac{\partial H_1}{\partial p}\right)_{p^{n+1}},\end{aligned}\tag{2.35}$$

where

$$c_1=0,\ c_2=c_4=\alpha,\ c_3=\beta,\ d_1=d_4=\frac{1}{2}\alpha,\ d_2=d_3=\frac{1}{2}(\alpha+\beta),\tag{2.36}$$

or

$$c_1=c_4=\frac{1}{2}\alpha,\ c_2=c_3=\frac{1}{2}(\alpha+\beta),\ d_1=d_3=\alpha,\ d_2=\beta,\ d_4=0,\tag{2.37}$$

and $\alpha=(2-\sqrt[3]{2})^{-1}$, $\beta=1-2\alpha$.

DOI https://doi.org/2007-CiCP-7894 | Generated on 2024-12-22 17:59:56
OPEN ACCESS

2.3.2 Explicit symplectic schemes for time-dependent Hamiltonian functions

In a quantum system, we often need to solve numerically the Hamiltonian system involving the time variable explicitly. The Hamiltonian function has the form

$$H(p,q,t)=H_1(p,t)+H_2(q,t). \tag{2.38}$$

The 1st-order explicit symplectic scheme

$$p^{n+1}=p^n-\tau\left(\frac{\partial H_2(q,t)}{\partial q}\right)_{(q^n,t_{n+\frac{1}{2}})},\quad q^{n+1}=q^n+\tau\left(\frac{\partial H_1(p,t)}{\partial p}\right)_{(p^{n+1},t_{n+\frac{1}{2}})}, \tag{2.39}$$

and the 2nd-order explicit symplectic scheme

$$\begin{aligned} &p_1=p^n, && q_1=q^n+\frac{\tau}{2}\left(\frac{\partial H_1(p,t)}{\partial p}\right)_{(p^n,t_{n+\frac{1}{2}})},\\ &p^{n+1}=p_1-\tau\left(\frac{\partial H_2(q,t)}{\partial q}\right)_{(q_1,t_{n+\frac{1}{2}})}, && q^{n+1}=q_1+\frac{\tau}{2}\left(\frac{\partial H_1(p,t)}{\partial p}\right)_{(p^{n+1},t_{n+\frac{1}{2}})} \end{aligned} \tag{2.40}$$

are tailored to the time-dependent Hamiltonian system (2.38), where $t_{n+\frac{1}{2}}=t_0+(n+1/2)\tau$.

We can use a simple technique [22] to construct high-order explicit symplectic schemes from known symplectic schemes. For example, the n-stage nth-order explicit symplectic scheme is of the form

$$\begin{aligned} &p_1=p^n-c_1\tau\left(\tfrac{\partial H_2(q,t)}{\partial q}\right)_{(q^n,t^n)}, && q_1=q^n+d_1\tau\left(\tfrac{\partial H_1(p,t)}{\partial p}\right)_{(p_1,\zeta_1)},\\ &\zeta_1=t^n+c_1\tau, && \xi_1=t^n+d_1\tau;\\ &p_2=p_1-c_2\tau\left(\tfrac{\partial H_2(q,t)}{\partial q}\right)_{(q_1,\xi_1)}, && q_2=q_1+d_2\tau\left(\tfrac{\partial H_1(p,t)}{\partial p}\right)_{(p_2,\zeta_2)},\\ &\zeta_2=\zeta_1+c_2\tau, && \xi_2=\xi_1+d_2\tau;\\ &p_3=p_2-c_3\tau\left(\tfrac{\partial H_2(q,t)}{\partial q}\right)_{(q_2,\xi_2)}, && q_3=q_2+d_3\tau\left(\tfrac{\partial H_1(p,t)}{\partial p}\right)_{(p_3,\zeta_3)},\\ &\zeta_3=\zeta_2+c_3\tau, && \xi_3=\xi_2+d_3\tau;\\ &\quad\vdots && \quad\vdots\\ &p^{n+1}=p_{n-1}-c_k\tau\left(\tfrac{\partial H_2(q,t)}{\partial q}\right)_{(q_{n-1},\xi_{n-1})}, && q^{n+1}=q_{n-1}+d_n\tau\left(\tfrac{\partial H_1(p,t)}{\partial p}\right)_{(p^{n+1},\zeta_n)},\\ &\zeta_n=\zeta_{n-1}+c_n\tau, && \xi_n=\xi_{n-1}+d_n\tau, \end{aligned}$$

where p_j,q_j,ξ_j,ζ_j, $j=1,\cdots,n$, are intermediate stages.

In a quantum system, we also need to solve the Hamiltonian system

$$H(p,q,t)=H_1(p)+H_2(q,t), \tag{2.41}$$

DOI https://doi.org/2007-CiCP-7894 | Generated on 2024-12-22 17:59:56
OPEN ACCESS

whose Hamiltonian equation is

$$\begin{cases} \dot{p}=-\dfrac{\partial H_2(q,t)}{\partial q}=-f(q,t), \\ \dot{q}=\dfrac{\partial H_1(p)}{\partial p}=g(p). \end{cases} \tag{2.42}$$

The following schemes can be used to solve numerically the Hamiltonian system (2.42).

- The 1st-order explicit symplectic scheme:

$$p^{n+1}=p^n-\tau f(q^n,t_n), \quad q^{n+1}=q^n+\tau g(p^{n+1}); \tag{2.43}$$

- The 2-stage, 2nd-order explicit symplectic scheme:

$$\begin{aligned} &p_1=p^n, \quad q_1=q^n+\frac{1}{2}\tau g(p_1), \quad \xi_1=t^n+\frac{1}{2}\tau, \\ &p^{n+1}=p_1-\tau f(q_1,\xi_1),\ q^{n+1}=q_1+\frac{1}{2}\tau g(p^{n+1}),\ t^{n+1}=\xi_1+\frac{1}{2}\tau; \end{aligned} \tag{2.44}$$

- The 4-stage, 4th-order explicit symplectic scheme:

$$\begin{aligned} &p_1=p^n-\tau c_1 f(q^n,t^n), && q_1=q^n+\tau d_1 g(p_1), && \xi_1=t^n+\tau d_1, \\ &p_2=p_1-\tau c_2 f(q_1,\xi_1), && q_2=q_1+\tau d_2 g(p_2), && \xi_2=\xi_1+\tau d_2, \\ &p_3=p_2-\tau c_3 f(q_2,\xi_2), && q_3=q_2+\tau d_3 g(p_3), && \xi_3=\xi_2+\tau d_3, \\ &p^{n+1}=p_3-\tau c_4 f(q_3,\xi_3), && q^{n+1}=q_3+\tau d_4 g(p^{n+1}), && t^{n+1}=\xi_3+\tau d_4, \end{aligned} \tag{2.45}$$

  where p_j,q_j,ξ_j, j=1,2,3, are intermediate stages, and the constants c_j and d_j are given by (2.36) or (2.37).

Sanz-Serna and Portillo [22] presented an s-stage, r-order partitioned Runge-Kutta method (PRK method):

$$\begin{aligned} &u_{n,0}=q^n, \quad v_{n,1}=p^n, \\ &u_{n,i}=u_{n,i-1}+\tau B_i g(v_{n,i}),\ v_{n,i+1}=v_{n,i}-\tau b_i f(u_{n,i},t_n+C_i\tau),\ 1\le i\le s; \\ &q^{n+1}=u_{n,s}, \quad p^{n+1}=v_{n,s+1}, \end{aligned} \tag{2.46}$$

where $u_{n,i}$ and $v_{n,i}$ are intermediate stages, b_i, B_i are constants, and $C_i=B_1+\cdots+B_i$. For example, for s=5 and r=4, i.e., the 5-stage, 4th-order PRK method, we have

$$\begin{aligned} &b_1=\frac{6}{11},\ b_2=\frac{1}{2}-b_1,\ b_3=b_2,\ b_4=b_1,\ b_5=0, \\ &B_1=\frac{1}{3924}(642+\sqrt{471}), \quad B_2=\frac{121}{3924}(12-\sqrt{471}), \\ &B_3=1-2(B_1+B_2), \quad B_4=B_2, \quad B_5=B_1. \end{aligned}$$

DOI https://doi.org/2007-CiCP-7894 | Generated on 2024-12-22 17:59:56
OPEN ACCESS

2.3.3 Symplectic scheme for general Hamiltonian system

For the general Hamiltonian system (2.10), the Euler-centered scheme

$$\frac{z^{n+1}-z^n}{\tau}=J^{-1}\left(\frac{\partial H}{\partial z}\right)_{(\frac{z^{n+1}+z^n}{2})} \tag{2.47}$$

is a 2nd-order implicit scheme. Feng [6] constructed symplectic schemes based on the generating function. For example, the 1st-order symplectic scheme is of the form

$$p^{n+1}=p^n-\tau\left(\frac{\partial H}{\partial q}\right)_{(p^{n+1},q^n)},\quad q^{n+1}=q^n+\tau\left(\frac{\partial H}{\partial p}\right)_{(p^{n+1},q^n)}; \tag{2.48}$$

and the 4th-order symplectic scheme is of the form

$$\frac{z^{n+1}-z^n}{\tau}=J^{-1}(\nabla H)_{(\frac{z^{n+1}+z^n}{2})}-\frac{\tau^2}{24}J^{-1}\nabla_z((\nabla H)^T JH_{zz}J\nabla H)_{(\frac{z^{n+1}+z^n}{2})}. \tag{2.49}$$

We rewrite equation (2.10) in the form

$$\dot{z}=J^{-1}\frac{\partial H}{\partial z}=f(z). \tag{2.50}$$

Sanz-Serna and Portillo [22] constructed a 2-stage, 4th-order implicit symplectic Runge-Kutta scheme,

$$\begin{aligned}
Y_1&=z^n+\tau\left(\frac{1}{4}f(Y_1)+\left(\frac{1}{4}-\frac{\sqrt{3}}{6}\right)f(Y_2)\right),\\
Y_2&=z^n+\tau\left(\left(\frac{1}{4}+\frac{\sqrt{3}}{6}\right)f(Y_1)+\frac{1}{4}f(Y_2)\right),\\
z^{n+1}&=z^n+\frac{\tau}{2}(f(Y_1)+f(Y_2));
\end{aligned} \tag{2.51}$$

and a 2-stage, 2nd-order implicit symplectic Runge-Kutta scheme,

$$\begin{aligned}
&Y_1=z^n+\frac{\tau}{2}f(Y_1),\quad Y_2=z^n+\frac{\tau}{2}f(Y_1)+\frac{\tau}{4}f(Y_2),\\
&z^{n+1}=z^n+\frac{\tau}{2}(f(Y_1)+f(Y_2)).
\end{aligned} \tag{2.52}$$

3 Classical dynamics of molecular system in an intense laser field

The classical trajectory method, in which the nuclei are assumed to move on the electronic potential energy surface of the molecular system, is an effective method to study micro-reaction, which requires to compute many classical trajectories. We point out that the symplectic algorithm is a more effective method in the calculation of the classical trajectories.

DOI https://doi.org/2007-CiCP-7894 | Generated on 2024-12-22 17:59:56
OPEN ACCESS

3.1 Classical trajectories for free-field molecular system

3.1.1 Classical theory and classical trajectory method

While the dimensionality of the molecular system becomes large, the quantum mechanical methods will be intractable in the study of molecular kinetics and dynamics. In this case, the classical method in which the nuclei move on the electronic potential energy surface of the molecular system is often adopted.

The classical trajectory method of the molecular dynamics study is conveniently divided into several steps. The first of these is the evaluation of the electronic potential energy surface of the given molecular system. Once the potential energy surface determined, the next task is to solve the Hamilton's equations of the molecular system because the classical mechanics are assumed to be valid for the motion of the nuclei on the potential energy surface. After a set of initial coordinates and momentum of the nuclei have been determined, a unique trajectory can be obtained by integrating the Hamilton's equations of motion. Since only a set of initial states selected is not reasonable in the experimental situation, all kinds of possible initial states of the molecular system considered must be calculated. After a large number of classical trajectories of the molecular system have been obtained, we may evaluate the measurable quantities of interest by the appropriate statistical average. In the following, we give a brief introduction to the methodology of the classical trajectory.

`Classical Equations of Motion.` The numerical integration of a set of differential equations are involved during the calculation of trajectories of the classical trajectory method. And the form of these equations depends on the choice of coordinates system. We give a brief introduction of the formulation of the equations of motion for N atom system in a generalized coordinate system.

With the Newton's second law, classical equations of motion can be expressed in the following form if a Cartesian coordinate system is adopted:

$$\frac{d}{dt}\left(\frac{\partial T}{\partial \dot{X}_i}\right)+\frac{\partial V}{\partial X_i}=0,\quad \frac{d}{dt}\left(\frac{\partial T}{\partial \dot{Y}_i}\right)+\frac{\partial V}{\partial Y_i}=0,\quad \frac{d}{dt}\left(\frac{\partial T}{\partial \dot{Z}_i}\right)+\frac{\partial V}{\partial Z_i}=0, \tag{3.1}$$

for $i=1,\cdots,N$, where (X_i,Y_i,Z_i) is the coordinate of the i^{th} atomic nucleus, V is the potential energy function of the N atom system, and the kinetic energy T of the system has the form

$$T=\frac{1}{2}\sum_{i=1}^{N} m_i(\dot{X}_i^2+\dot{Y}_i^2+\dot{Z}_i^2). \tag{3.2}$$

Obviously, (3.1) is a set of $3N$ second-order differential equation of motion in the Cartesian coordinates. In many cases, Eq. (3.1) is directly applicable to the problem if the adopted coordinate system is the Cartesian one. However, it is more convenient to employ a generalized coordinate system when the given system contains three atoms or less. By an appropriate set of transformation equations, Eq. (3.1) can be transformed into Lagrangian form applicable to any set of generalized coordinates. Since a set of first-order

DOI https://doi.org/2007-CiCP-7894 | Generated on 2024-12-22 17:59:56
OPEN ACCESS

differential equations facilitates the numerical solution during the computation of classical trajectories, the Hamiltonian form of the equations of motion is often introduced.

The classical Hamiltonian is defined by $H=T+V$, and we have the Hamilton's equations of motion,

$$\dot{p}_i=-\frac{\partial H}{\partial q_i},\quad \dot{q}_i=\frac{\partial H}{\partial p_i},\quad i=1,\cdots,3N. \tag{3.3}$$

Eq. (3.3) is a set of $6N$ first-order differential equations known as *Hamilton's equations* that constitute the working equations for most trajectory calculations.

Selection of initial conditions. In the classical trajectory study, all kinds of possible initial states corresponding to the experimental situation for the N atoms system have to be involved. In such a case, the Monte Carlo statistical average is often adopted to yield a large number of initial states of N atom systems. As a matter of fact, the Monte Carlo procedure is the only practical approach to simulate the average properties of classical trajectories of the given system.

Evaluation of the measurable attributes. After all kinds of possible initial states are selected by the Monte Carlo procedures, we can obtain a large number of classical trajectories of the given system. The measurable attributes of interest of the system can be evaluated by the appropriate statistical average of all classical trajectories.

For example, the reaction probability of the atom-molecule reaction system can be determined from the equation

$$Pb(b,v,J,Et)=\lim_{N\to\infty}\frac{Nr(b,v,J,Et)}{N(b,v,J,Et)},$$

where b is the impact parameter, v is the vibrational level of the reactant molecule, J is the rotational level of the reactant molecule, Et is the relative translational energy, $Nr(b,v,J,Et)$ and $N(b,v,J,Et)$ are the numbers of reactive trajectories and total trajectories, respectively. When we fix the initial condition set (b,v,J,Et), with the values of other variables selected randomly by the Monte Carlo procedure, the corresponding reaction probability of the atom-molecule reaction system can be calculated by the above equation. With the knowledge of $Pb(b,v,J,Et)$, the total reaction cross-section $Sr(v,J,Et)$ can be determined by the equation

$$Sr(v,J,Et)=\pi b_{\max}^2(v,J,Et)[Nr(v,J,Et)/N(v,J,Et)],$$

where $Nr(v,J,Et)$ and $N(v,J,Et)$ are the numbers of reactive collisions and total collisions at a given set of initial conditions (v,J,Et), respectively, and $b_{\max}(v,J,Et)$ is the maximal impact parameter.

3.1.2 Diatomic molecular system

Consider the classical motion of a diatomic molecule AB in the electronic potential, where the mass of atom A is m_1 and the mass of atom B is m_2. The coordinates of A and B

DOI https://doi.org/2007-CiCP-7894 | Generated on 2024-12-22 17:59:56
OPEN ACCESS

are x_1 and $-x_2$, respectively. Suppose $q=R=x_1+x_2$ is the canonical coordinate, $\mu=(m_1+m_2)/(m_1m_2)$ is the canonical mass. Then $p=\mu q_t$ and $U=p^2/(2\mu)$ are the canonical momentum and canonical kinetic, respectively. The Morse potential is

$$V(q)=D_e\{1-\exp(-\alpha(q-q_0))\}^2,$$

while the Murrell-Sorbie potential is

$$V(q)=-D\Big\{1+\sum_k a_k(q-q_e)^k e^{-a_1(q-q_e)}\Big\}.$$

The total energy of the diatomic molecule AB system is

$$H(p,q)=U(p)+V(q)=\frac{1}{2\mu}p^2+V(q), \tag{3.4}$$

and the classical Hamiltonian canonical equation is

$$\begin{aligned}\frac{dp}{dt}&=-\frac{\partial H}{\partial q}=-\frac{\partial V}{\partial q},\\ \frac{dq}{dt}&=\frac{\partial H}{\partial p}=\frac{\partial U}{\partial p}=\frac{p}{\mu}.\end{aligned} \tag{3.5}$$

Since (3.5) is a separated Hamiltonian system, an explicit symplectic scheme can be used to solve this system, for example, the explicit symplectic scheme (2.30)-(2.35).

We fit the potential parameters to the HF molecule in the Morse potential, such that $D_e=0.225$, $\alpha=1.1741$, $q_0=1.7329$ and $\mu=1744.8423$, where atomic units are used unless otherwise stated. This potential supports 24 bound vibrational levels for the HF molecule, i.e $\nu=0,1,\cdots,23$.

Fig. 2 shows the evolution of the energy and the nuclei separation versus time without laser pulse. Fig. 2(a) indicates that the energy is conserved, while Fig. 2(b) indicates that two atoms oscillate periodically in the evolution process. Fig. 3 depicts the phase trajectories of free HF molecule in phase space R-P. We can see from Fig. 3 that the phase trajectories in phase space are steady, which is in good agreement with the theoretic analysis.

3.1.3 Model molecule A_2B

Banerjee and Adams [45] constructed a transformation in a straightforward way to yield a set of active and redundant coordinates in which the Hamiltonian equations are separable. For an N-particle system with Hamiltonian function $H=H(p_i,q_i)$, $1\le i\le 3N$, the corresponding Hamiltonian equations are

$$\dot{p}_i=-\frac{\partial H}{\partial q_i},\qquad \dot{q}_i=\frac{\partial H}{\partial p_i},$$

DOI https://doi.org/2007-CiCP-7894 | Generated on 2024-12-22 17:59:56
OPEN ACCESS

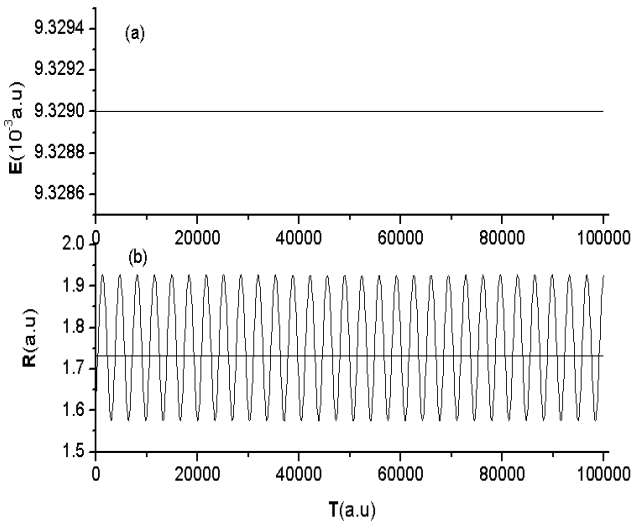

Figure 2: The evolution of the energy and the nuclei separation without pulse. (a) The evolution of the energy; (b) The evolution of the nuclei separation versus time, where the middle line represents the equilibrium nuclei separation R_0.

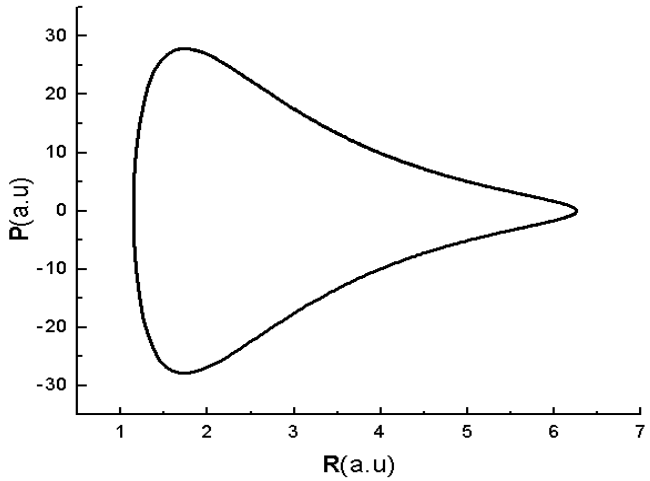

Figure 3: Phase trajectories of free HF molecule in the phase space R-P.

where q_i is the canonical coordinate, and p_i is the canonical momentum. The kinetic energy has the form $T = p^T M^{-1} p/2$, where $p = (p_1, \cdots, p_n)^T$, M^{-1} is the mass matrix which is a diagonal matrix formed by the mass of N-particle. The potential energy has the form $V = V(q)$, which is only a function of coordinate, where $q = (q_1, \cdots, q_n)^T$. From the canonical transformation $Q = T^{-1} q$, $P = T^T p$ and independent relations $\partial H/\partial q_\alpha = C \partial H/\partial q_i$ obtained by the symmetry relation [45], the coordinates can be separated into active and

DOI https://doi.org/2007-CiCP-7894 | Generated on 2024-12-22 17:59:56
OPEN ACCESS

cyclic coordinates. In such way, we can obtain the generalized coordinate

$$Q_i = q_i + C^T q_\alpha = q_i + C_{i\alpha} q_\alpha, \tag{3.6}$$

and the generalized mass

$$\Omega_{ii}^{-1} = m_{ii}^{-1} + C^T m_{\alpha\alpha}^{-1} C, \tag{3.7}$$

where the mass matrix $M^{-1} = \mathrm{diag}(m_{ii}^{-1}, m_{\alpha\alpha}^{-1})$ is block diagonal.

Consider the motion of the model of an A_2B type molecule within the C_{2v} symmetry. Suppose the mass of atom A and atom B is $m_1 = 1$ and $m_2 = 2$, respectively. The atom B is labeled particle 1, and the two A atoms are labeled 2 and 3, respectively. We constructed the Cartesian coordinate system yOz, with origin at the center of mass O, and the z axis is the C_2 axis. Denote the coordinates of the two A atoms and atom B by $A(y_1, z_1)$, $A(y_2, z_2)$ and $B(y_3, z_3)$, respectively. The potential energy function is given by

$$\begin{aligned} V = {} & 10\pi^2 \left\{ f(\triangle) \left[(r_{12}-1)^2 + (r_{13}-3/2)^2 \right] + f(-\triangle) \left[(r_{12}-1)^2 + (r_{13}-3/2)^2 \right] \right\} \\ & + \frac{1}{2\pi^2} (r_{23}-3/2)^2 + \frac{1}{r_{12}} + \frac{1}{r_{13}} + \frac{1}{r_{23}}, \end{aligned} \tag{3.8}$$

where $\triangle = 5(r_{12} - r_{13})$, $f(\triangle) = (1 + \tanh(\triangle))/2$, and r_{ij} $(i,j = 1,2,3)$ is the internuclear distance. With the C_{2v} symmetry and (3.6)-(3.7), we can obtain the generalized coordinates

$$Q_1 = z_1 - 2z_3 + z_2, \qquad Q_2 = y_1 - y_2, \tag{3.9}$$

and the generalized mass

$$\Omega_1 = (2/m_1 + 4/m_2)^{-1} = \frac{1}{4}, \quad \Omega_2 = (2/m_1)^{-1} = \frac{1}{2}, \tag{3.10}$$

such that the Hamiltonian function of the A_2B type molecule is

$$H(P,Q) = K(P) + V(Q), \tag{3.11}$$

where the kinetic energy and potential energy are given by

$$\begin{aligned} & K(P) = 2P_1^2 + P_2^2, \\ & V(Q) = 5\pi^2 \left(D^2 - 5D + \frac{13}{2} \right) + \frac{4}{D} + \frac{\pi^2}{2} \left(|Q_2| - \frac{3}{2} \right)^2 + \frac{1}{|Q_2|}, \end{aligned} \tag{3.12}$$

respectively. Here the generalized momentum $P_1 = (1/4) dQ_1/dt$, $P_2 = (1/2) dQ_2/dt$ and $D = \sqrt{Q_1^2 + Q_2^2}$. The canonical equation of classical motion is

$$\dot{P}_i = -\frac{\partial V}{\partial Q_i} = -f_i(Q_1, Q_2), \quad \dot{Q}_i = \frac{\partial K}{\partial P_i} = g_i(P_1, P_2), \; i = 1,2, \tag{3.13}$$

DOI https://doi.org/2007-CiCP-7894 | Generated on 2024-12-22 17:59:56
OPEN ACCESS

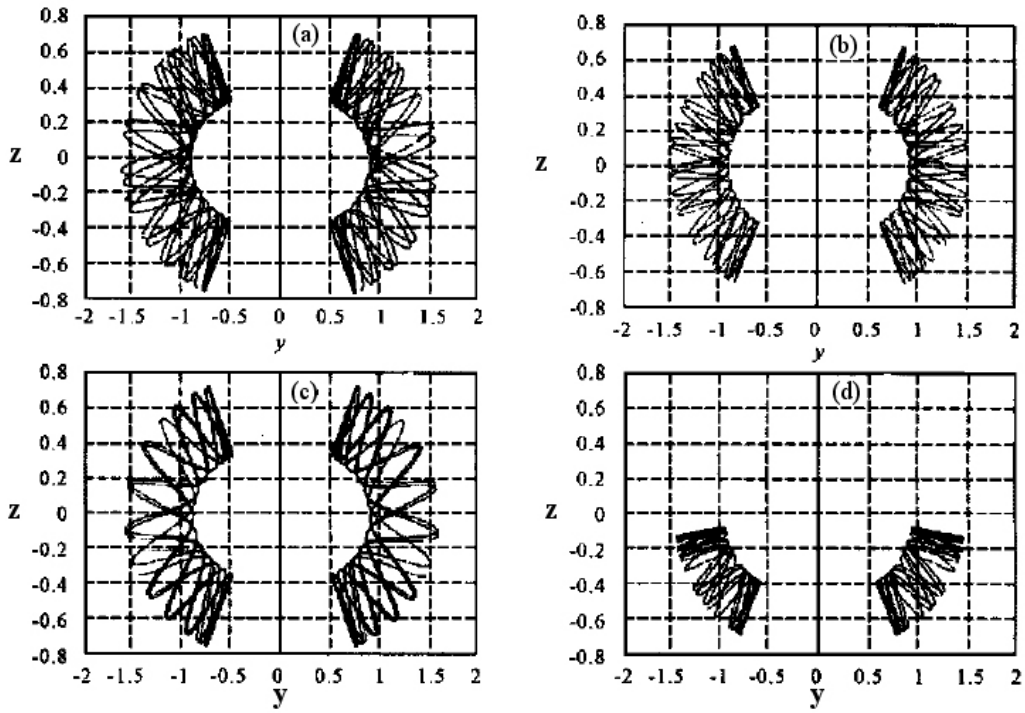

Figure 4: Classical trajectories in phase space: (a) and (c) are obtained by using a symplectic method; and (b) and (d) are obtained by using a Runge Kutta method.

where

$$f_1(Q_1,Q_2)=5\pi^2Q_1(2-5/D)-4Q_1/D^3,\quad g_1(P_1,P_2)=4P_1,\quad g_2(P_1,P_2)=2P_2,$$

$$f_2(Q_1,Q_2)=5\pi^2Q_2(2-5/D)-4Q_2/D^3+\begin{cases}\pi^2(Q_2-3/2)-Q_2^{-2} & \text{if } Q_2>0,\\ \pi^2(Q_2+3/2)+Q_2^{-2} & \text{if } Q_2<0.\end{cases}$$

This Hamiltonian system is separable, which can be solved by the explicit symplectic schemes (2.30)-(2.32). Fig. 4 shows the classical trajectories of an A_2B type molecule in phase spaces, obtained by using a symplectic method and a Runge-Kutta method, respectively. It is observed from Fig. 4 that the numerical results computed by the symplectic method are in good agreement with the theoretical analysis; the atom B and two atoms A in A_2B type molecule vibrate quasi-periodically. However, the numerical results computed by the Runge-Kutta method are not in agreement with the theoretical analysis; the vibrational range of A_2B type molecule shrinks [46].

Fig. 5 shows the energy evolutions computed by symplectic method and the Runge-Kutta method. The total energy computed by the symplectic method is consistent with the physical analysis, but that from Runge-Kutta is unpredictable.

The above computations indicate that the symplectic algorithm is a class of difference method that preserves the symplectic structure, and is a reliable method for long time simulations of the classical trajectories.

DOI https://doi.org/2007-CiCP-7894 | Generated on 2024-12-22 17:59:56
OPEN ACCESS

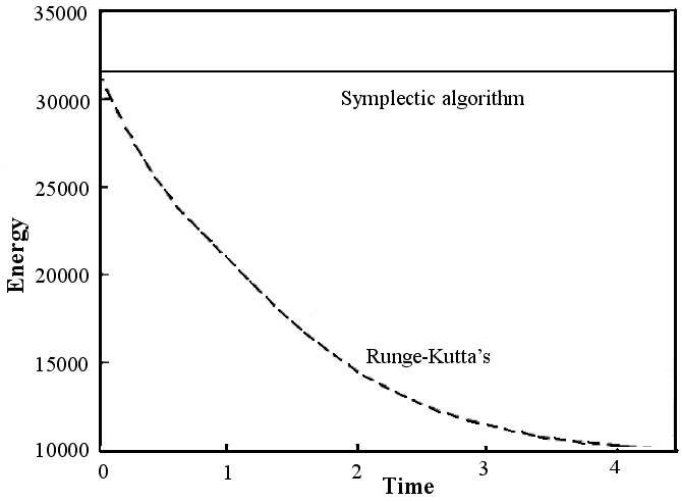

Figure 5: Comparison of the energy evolutions.

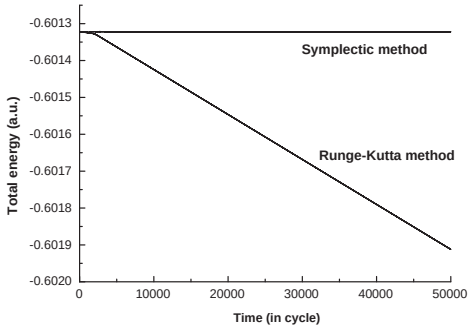

Figure 6: The evolution of the total energy in free-field by using a symplectic method and a Runge-Kutta method.

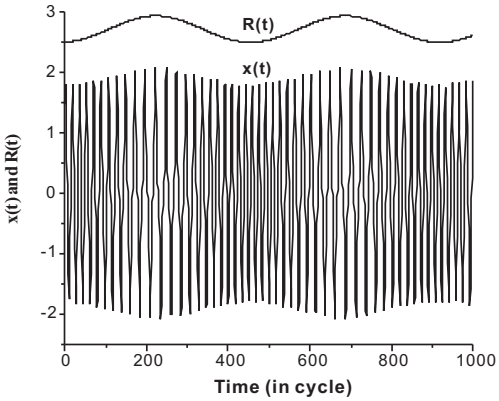

Figure 7: The evolution of the electronic position and the internuclear distance in free-field by using a symplectic method.

3.1.4 Hydrogen molecular ion H_2^+

The two protons and electron in H_2^+ system can be regarded as the classical particles based on the classical theory. The system of H_2^+ is regarded as a three-body system of classical mechanics. The classical movement of system is described by the Hamiltonian canonical equation. The Hamiltonian function of H_2^+ can be written as

$$H(P,p;x,R)=\frac{P^2}{2\mu_p}+\frac{p^2}{2\mu_e}+V_c(x,R), \tag{3.14}$$

where $\mu_p=m_p/2$, $\mu_e=2m_em_p/(2m_p+m_e)$ are the reduced masses, m_p, m_e are the proton and electron masses, respectively. R is the internuclear distance of two protons and P is its

DOI https://doi.org/2007-CiCP-7894 | Generated on 2024-12-22 17:59:56
OPEN ACCESS

corresponding conjugated momentum, while x is the distance between the electron and the center of the mass of two protons, and p is its corresponding conjugated momentum. The screened Coulomb potential is

$$V_c(x,R)=\frac{1}{R}-\Big((x-R/2)^2+q_e\Big)^{-1/2}-\Big((x+R/2)^2+q_e\Big)^{-1/2},$$

where the parameter q_e (we choose q_e=1 a.u.) is the screened parameter of the 1D Coulomb potential.

We give an initial energy $E_0=-0.78$ a.u.. Fig. 6 indicates that the evolution of the total energy in the free-field can be preserved for long-time computation by using a symplectic method, but the evolution of the total energy decreases rapidly for long-time computation when using Runge-Kutta method. We show the evolution of the electronic position and the internuclear distance obtained by using the symplectic method in Fig. 7. The electron and nuclear oscillate periodically near the balanced position which illustrates that the system remains stable when using the symplectic method.

3.1.5 Chemical reaction system

We studied the elementary atmospheric reaction [47,48], $N(^4S)+O_2(X^3\Sigma_g^-)\rightarrow NO(X^2\Pi)+O(^3P)$, which plays an important role in the Earth's atmospheric chemistry. This reaction is a source of infrared chemiluminescence in the thermosphere [49]. High temperature studies of kinetics and dynamics of the atmospheric reaction and its reverse are also significant to interpret the chemical and physical phenomena taking place during the reentry of spacecrafts into the Earth's atmosphere [50].

In the atom-molecule (A+BC) reaction system, the masses of atoms A, B and C are denoted by m_A, m_B and m_C, respectively. In the present case, A is taken to be the nitrogen atom (N), B is the first oxygen atom (O) and C is the second oxygen atom (O). Because the reaction system has no outfield action, the momentum of the reaction system is constant. Separating out the center-of-mass motion, we write the internal Hamiltonian in the form

$$H=\frac{1}{2\mu_{B,C}}\sum_{j=1}^{3}P_j^2+\frac{1}{2\mu_{A,BC}}\sum_{j=4}^{6}P_j^2+V(Q_1,...,Q_6), \tag{3.15}$$

where Q_j $(1\leq j\leq 6)$ represents the generalized Cartesian coordinate, P_j $(1\leq j\leq 6)$ is the momentum conjugate to the Q_j, $V(Q_1,\cdots,Q_6)$ is the potential energy function, and the reduced masses are $\mu_{B,C}=m_Bm_C/(m_B+m_C)$ $\mu_{A,BC}=m_A(m_B+m_C)/(m_A+m_B+m_C)$.

Numerous quasiclassical trajectories, based on the new ground PES reported by R. Sayós et al. [51], have been calculated by means of the 4th-order explicit symplectic algorithm (S4) for the atmospheric reaction, and then the result is compared to that computed by the 4th-order Runge-Kutta scheme (RK4). Fig. 8 depicts the comparison of the total energy evolving with the time computed by S4 and RK4, respectively. It is observed from Fig. 8(a) that the total energy of the reaction system calculated by RK4 decreases with the time. This reveals that the deviation of the total energy will become larger if

DOI https://doi.org/2007-CiCP-7894 | Generated on 2024-12-22 17:59:56
OPEN ACCESS

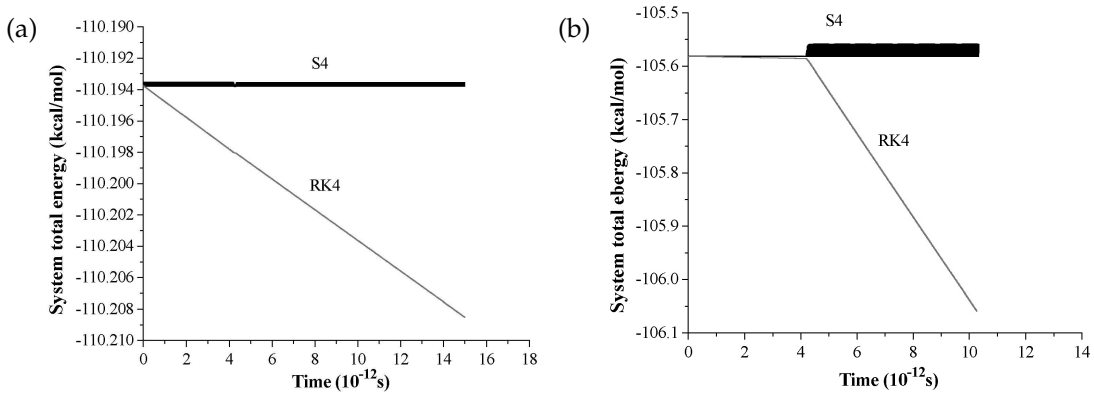

Figure 8: Comparison of total energies evolving with the time computed, respectively, by S4 and RK4: (a) Et=0.3eV, v=0, J=8, h=5.0×10^{-16}s (non-reaction), (b) Et=0.5eV, v=0, J=8, h=5.0×10^{-16}s (reaction).

the time is longer. The phenomenon in Fig. 8(a) is accounted for that the deviation of total energy adds in value with the time since the truncation error continuously accumulates during the integration. Except that the total energy computed by S4 oscillates slightly near the exact value, however, it is almost a constant. Since a reaction takes place in Fig. 8(b), its phenomenon is a little different from that in Fig. 8(a). The curve of total energy evolving with the time computed by RK4 in the product part has a larger slope than that in the reactant part, and the vibrating of total energy computed by S4 in the product part is clearly larger than that in the reactant part. The reason is that deviation of total energy is determined by the potential energy curve of the O_2 molecule before the reaction and by that of the NO molecule after the reaction.

Since RK4 cannot preserve the energy conservation and the symplectic structure of the reaction system, the trajectories computed by RK4 have some obvious differences from those computed by S4 under the same condition. Fig. 9 shows the comparison of some typical trajectories, where RHO denotes the initial distance between the N atom and the O_2 molecule in a.u., Et denotes the relative transnational energy in eV, h is the time step size in seconds, v and J represent, respectively, the vibrational and rotational level of O_2 molecule, R is the separation distance of the nuclei and the energy unit is taken to be kcal/mol. The trajectories computed by RK4 in Fig. 9(a) clarify that no reaction occurs although the collision goes through a transition state. Moreover, after the O_2 molecule collides with the N atom, the period and amplitude of vibration of the O_2 molecule become large. From Fig. 9(b), however, we see that a reaction that produces the NO molecule takes place. It is concluded that the loss of total energy may influence the colliding mode of the trajectories. Two differences exist between Figs. 9(c) and (d) that display the trajectories computed by RK4 and S4, respectively. One is the reaction mode, that is, Fig. 9 (c) is a direct reaction and Fig. 9(d) is an indirect reaction. Another is that the product in Fig. 9(c) is the NO molecule (the first oxygen atom) and there is a different NO molecule (the second oxygen atom) in Fig. 9(d).

DOI https://doi.org/2007-CiCP-7894 | Generated on 2024-12-22 17:59:56
OPEN ACCESS

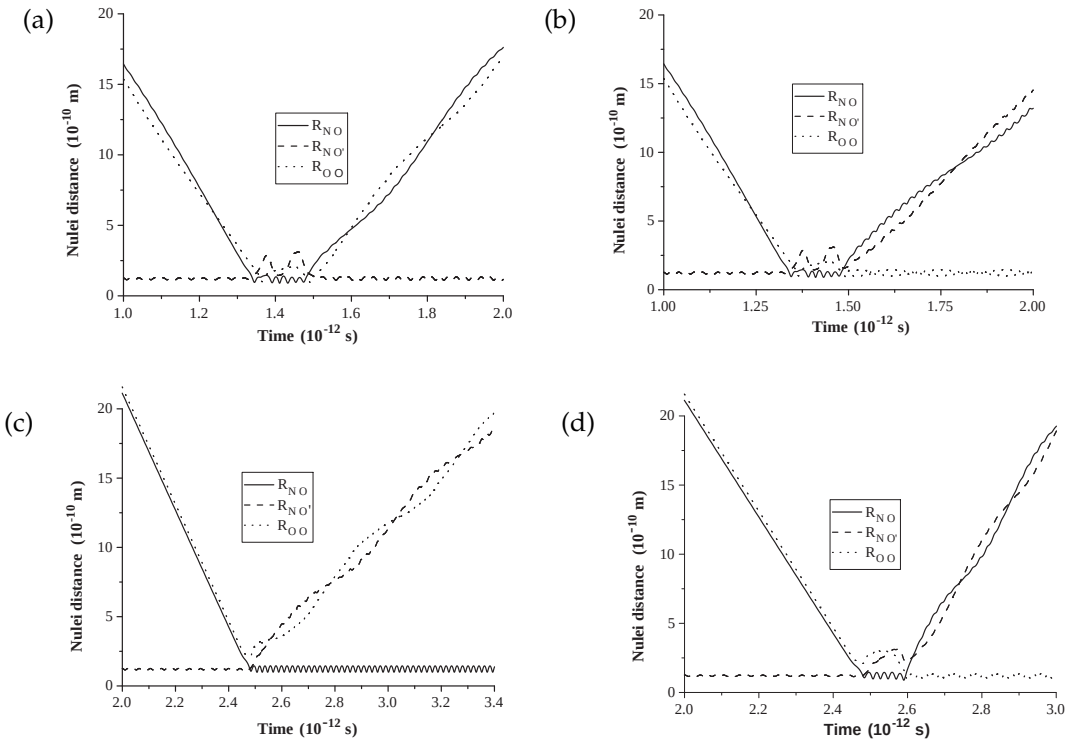

Figure 9: Comparison of trajectories evolving with time computed respectively by RK4 and S4. (a) Et=0.9eV, v=0, J=16, RHO=110.0a.u., h=4.0×10^{-16}s (by RK4). (b) Et=0.9eV, v=0, J=16, RHO=110.0a.u., h=4.0×10^{-16}s (by S4). (c) Et=0.9eV, v=0, J=0, RHO=220.0a.u., h=7.5×10^{-16}s (by RK4). (d) Et=0.9eV, v=0, J=0, RHO=220.0a.u., h=7.5×10^{-16}s (by S4).

We calculate a large number of quasiclassical trajectories by S4 for the atmospheric reaction, and some typical trajectories are presented in Fig. 10 at different relative translational energies, rotational and vibrational energy levels of the O_2 molecule. Fig. 10 (a) and Fig. 10(b) show the typical trajectories proceeding through an indirect mechanism. The N atom links with the first oxygen atom to make the NO molecule in Fig. 10(a), however, the reaction product in Fig. 10(b) consists of the N atom and the second oxygen atom. The typical trajectories in a direct mechanism are manifested in Fig. 10(c). The N atom approaches continuously to the O_2 molecule, in such a way that the vibrational level of the O_2 molecule is not influenced by the incoming N atom until the NO bond distance is almost reached. When the NO molecule is formed, the O-O distance grows fast. With no reaction occurs, Fig. 10(d) displays a typical elastic collision, where the period and amplitude of the vibration of O_2 molecule have no variation after the N atom collides with O_2 molecule. The inelastic collision that changes the internal energy of O_2 molecule also exists, but for simplicity we do not exhibit it.

Fig. 11(a) demonstrates the dependence of the reaction probability $Pb(b,v,J,Et)$ on the

DOI https://doi.org/2007-CiCP-7894 | Generated on 2024-12-22 17:59:56
OPEN ACCESS

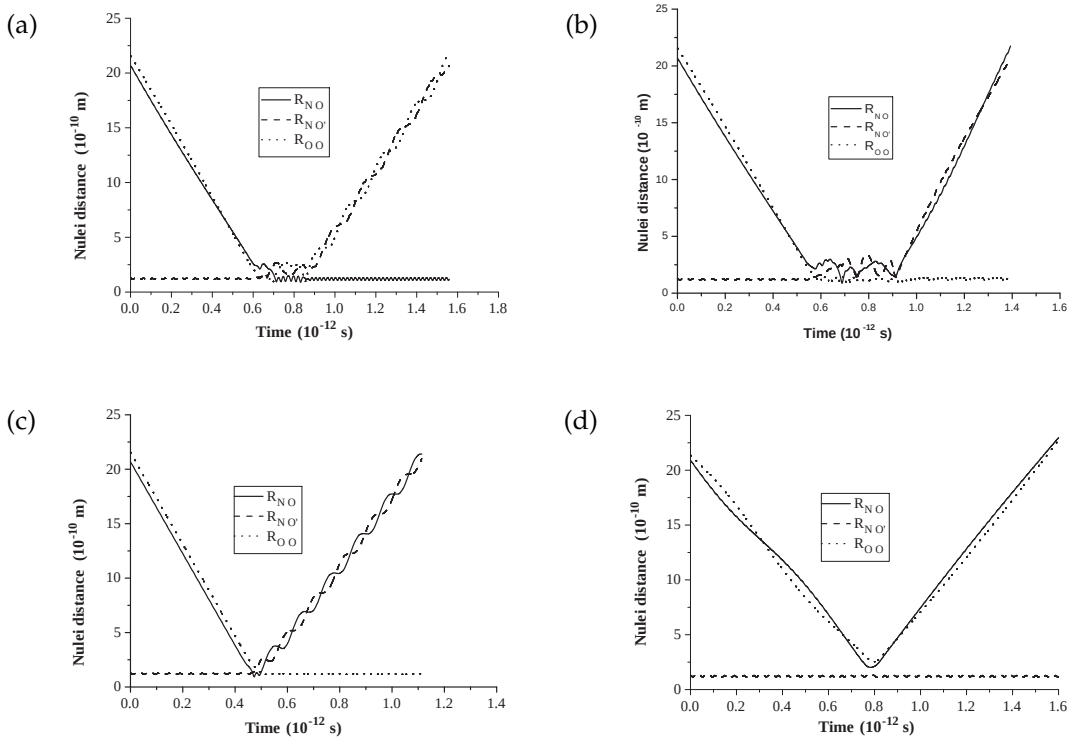

Figure 10: Typical trajectories and reactive mode analysis at h=1.0×10^{-16}s and RHO=40.0a.u. (a) Et=0.5eV, v=0, J=8 (b) Et=0.6eV, v=0, J=8 (c) Et=0.9eV, v=0, J=0 (d) Et=0.3eV, v=0, J=16.

impact parameter at different relative translational energies. As depicted by Fig. 11(a), the reaction probability reveals a declining trend as the impact parameter moves from 0 to its maximum with an increment of 0.15 Å. Except that both maximal impact parameters $b_{\max}(v,J,Et)$ and the areas under these curves of $Pb(b,v,J,Et)$ versus b associated with the relative translational energy, the shapes of these curves seem to be similar for all relative translational energies. It is also obvious in Fig. 11 (a) that the reaction probability as a function of the relative translational energy exhibits an increasing behavior above the threshold energy. The comparison of reaction probabilities of several rovibrational levels of the O_2 molecule has been displayed in Fig. 11(b), which indicates that the reaction probability is primarily independent of the initial rovibrational level of the O_2 molecule. This is due to the O_2 molecule remaining almost rotationally frozen, that is, the rotational period of the O_2 molecule is much larger than the corresponding transition time, so that the O_2 molecule does not have enough time to rotate in the course of the N atom interacting strongly with the O_2 molecule, as pointed out by Sayós et al. [52, 53].

Fig. 12 describes the variation of the total reaction cross-section with the relative translational energy. As depicted by Fig. 12, the total reaction cross-section enhances rapidly

DOI https://doi.org/2007-CiCP-7894 | Generated on 2024-12-22 17:59:56
OPEN ACCESS

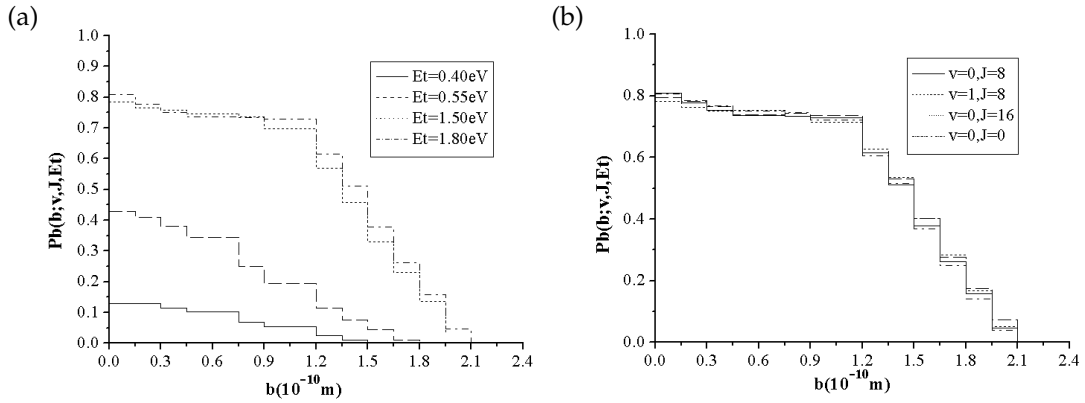

Figure 11: Variation of the reaction probability with the impact parameter. (a) at different relative translational energies with O_2 molecule in the v=0, J=8 level; (b) at different vibrational levels of O_2 molecule in Et=1.8eV.

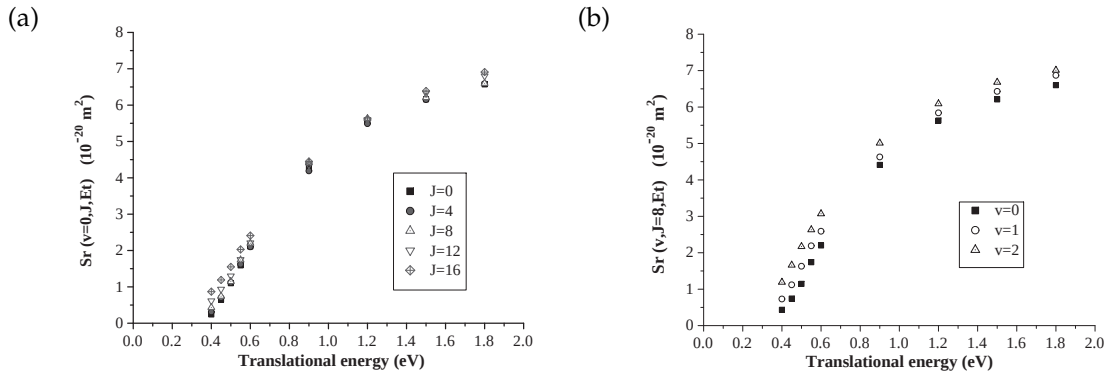

Figure 12: Variation of the total reaction cross-section with the relative translational energy. (a) O_2 molecule at v=0 and J=0, 4, 8, 12, 16; (b) O_2 molecule at J=8 and v=0, 1, 2.

with the relative translational energy above the energy threshold. From Fig. 12(a), the influence of the rotational level with the O_2 molecule at v=0 on the total reaction cross-section can also be analyzed. At low relative translational energy (less than 0.60 eV), the total reaction cross-section increases with the rotational level of the O_2 molecule. Although the absolute increments of the total reaction cross-section are fairly small, they have significant values with respect to the total reaction cross-section at the rovibrational level (v=0, J=0) of the O_2 molecule. However, the rotational level of the O_2 molecule plays an inconspicuous role in enhancing the total reaction cross-section at the higher relative translational energy. Fig. 12(b) displays the variation of the total reaction cross-section as the vibrational level of the O_2 molecule ranges from 0 to 2. It is apparent that the vibrational level of the O_2 molecule contributes modestly to the enhancement of the total reaction cross-section. The moderate effect of the vibrational level is due to the new PES with an early barrier employed in this work.

DOI https://doi.org/2007-CiCP-7894 | Generated on 2024-12-22 17:59:56
OPEN ACCESS

3.2 The classical dissociation of HF molecule by intense laser pulse

The Hamiltonian function of HF in external intense laser fields can be written as ([54,55])

$$H(P,R)=P^2/2\mu+V(R)-q_e\cdot E(t)\cdot R, \tag{3.16}$$

where $E(t)$ is the laser field, the effective charge q_e can be chosen as $[\partial D_p(R)/\partial R]|_{R=R_0}=0.31$, and $D_p(R)$ is the dipole moment. Moreover, $E(t)=E_m U(t)\sin(\Omega_c(t)\cdot t)$, where $\Omega_c=\Omega_\nu[1-\alpha_l(t/T_0)^l]$ with l=1,α_l=0.5, Ω_υ=1.1$\omega_{\nu,\nu+1}$, $\omega_{\nu,\nu+1}$ denoting the resonant frequency from $\nu\rightarrow\nu+1$. The period of the laser is $2\pi/\Omega_\nu$, and

$$U(t)=\begin{cases} t/t_0 & (t\leq t_0). \\ 1 & (t_0<t<T_0-t_0), \\ (T_0-t)/t_0 & (T_0-t_0<t\leq T_0). \end{cases} \tag{3.17}$$

We choose a vibrational state E_ν as the initial input, solve numerically the Hamiltonian equation in the free-field, and then select a set of trajectories (R_0,P_0) of the free-field as initial conditions in the external intense laser fields. Under these initial conditions we can solve numerically the Hamiltonian equation of HF in external intense laser fields. Consequently we can obtain a variety of trajectories which can be used to compute the dissociation probabilities.

Fig. 13 shows the changes of dissociation probabilities versus the laser intensity E_m. We select some different vibrational states ($\nu=3$, 8, 9, 15) as the initial input. Fig. 13 indicates that the larger the value of ν is, the smaller the laser intensity is needed to open the channel of dissociation. Fig. 14 shows the changes of the dissociation probabilities for different vibrational-rotational states as the initial input versus time with field strength $E_m=10^{13}W/cm^2$. We choose the vibrational-rotational states ($\nu=0$, $J=1$), ($\nu=3$, $J=1$), (ν=9, J=1), (ν=15, J=1) as the initial inputs. A comparison between the vibrational transitional dissociation and the vibrational-rotational transitional dissociation is also made in Fig. 14.

3.3 Classical dynamics of H_2^+ in an intense laser field

In this subsection we will study the interaction of 1D H_2^+ in an intense laser pulse by using the classical theory, and discuss the dynamical processes of survival, dissociation, ionization and Coulomb explosion of H_2^+ for different laser intensity. The external laser field is $E(t)=E_0 f(t)\sin\omega_0 t$, and $f(t)=\sin^2(\pi t/20T)$ when $0<t<T_D$ and $f(t)=0$ otherwise. We presume that the laser electric field is along the direction of two protons and adopt the 1D model in which the electron is collinear with two protons. Then the Hamiltonian function of H_2^+ in the external intense laser fields can be written as [56]

$$H(P,p;x,R,t)=\frac{P^2}{2\mu_p}+\frac{p^2}{2\mu_e}+V_c(x,R)+V_{ex}(x,t). \tag{3.18}$$

DOI https://doi.org/2007-CiCP-7894 | Generated on 2024-12-22 17:59:56
OPEN ACCESS

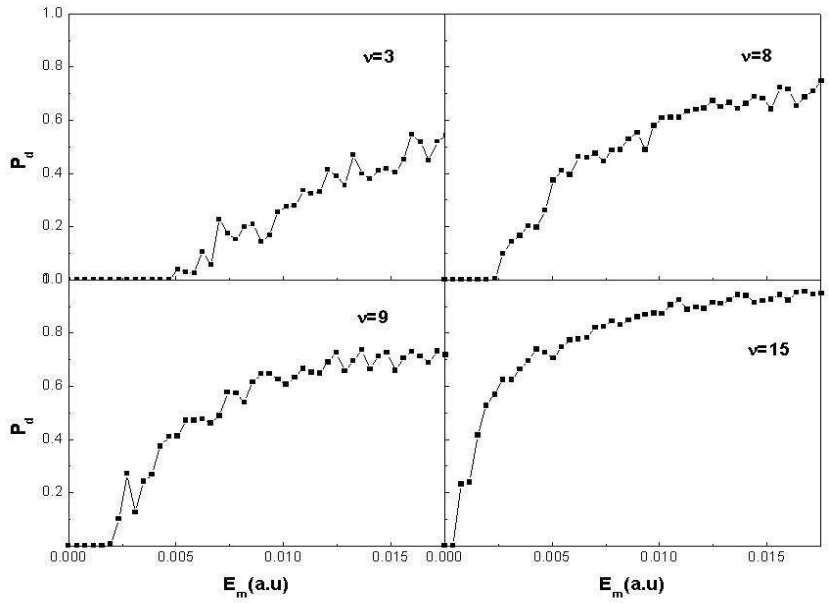

Figure 13: The changes of dissociation probabilities for different vibrational states as the initial input versus laser intensity E_m with interaction time $T_0=120$ cycles, $l=1$, $\alpha_l=0.5$.

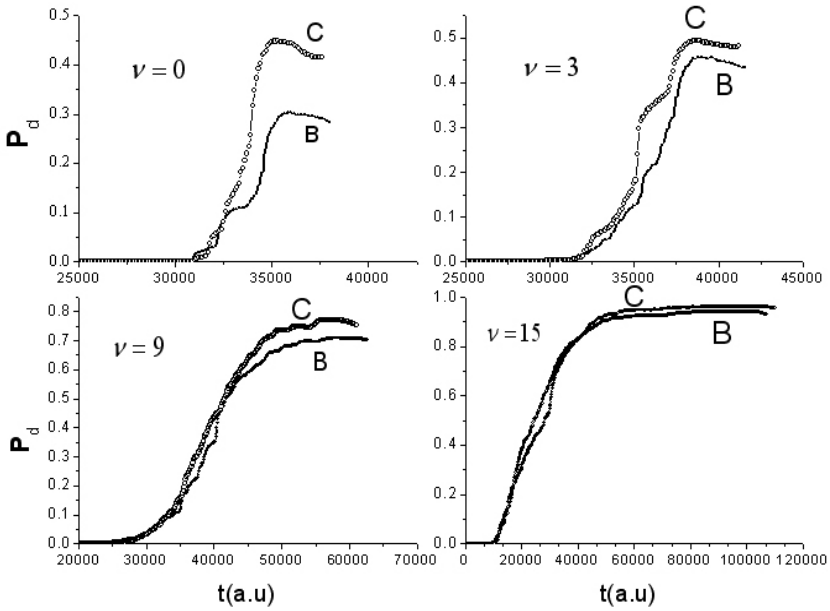

Figure 14: The changes of dissociation probabilities for different vibrational-rotational states ($\nu=0$, $J=1$; $\nu=3$, $J=1$; $\nu=9$, $J=1$; and $\nu=15$, $J=1$) as the initial input versus time with field strength ($E_m=10^{13}W/cm^2$), B denote the vibrational transitional dissociation, C denote the vibrational-rotational transitional dissociation.

DOI https://doi.org/2007-CiCP-7894 | Generated on 2024-12-22 17:59:56
OPEN ACCESS

The interaction potential with the external laser field is

$$V_{ex}(x,t) = -\sigma x E(t), \quad \sigma = 2(m_p+m_e)/(2m_p+m_e). \tag{3.19}$$

The total energy is [57]

$$E_c(t) = V_p + \frac{1}{2\mu_e}(\mu_e \dot{x}(t) - \sigma \int_0^t E(t')dt')^2, \tag{3.20}$$

where $V_p = V_c(x,R) - 1/R$ is the Coulomb potential experienced by an electron. During the course of system evolution, the electron is ionized when the total-energy $E_c(t) > 0$ and two nuclei are dissociated when the distance between two protons $R(t) > R_D = 10.0$a.u. (R_D is the largest internuclear distance) [58]. According to the above two criteria, four processes or channels may occur at any time interval during the interaction of H_2^+ with the laser pulses:

$$\begin{aligned}
&H_2^+ + [I] \to H_2^+ (E_c(t) \le 0, R(t) \le R_D), \\
&H_2^+ + [I] \to H + H^+ (E_c(t) \le 0, R(t) > R_D), \\
&H_2^+ + [I] \to H_2^{2+} + e (E_c(t) > 0, R(t) \le R_D), \\
&H_2^+ + [I] \to 2H^+ + e (E_c(t) > 0, R(t) > R_D),
\end{aligned} \tag{3.21}$$

where $[I]$ stands for the interaction of the laser pulse. We refer to above dynamic processes as survival, dissociation, ionization and Coulomb explosion of H_2^+, respectively.

We can select the initial condition by using a single trajectory in the field-free case at random in time intervals. Under these initial conditions we can solve numerically the Hamiltonian equation of H_2^+ in the external intense laser fields and obtain a variety of trajectories, which can be used to compute the four dynamic processes (survival, dissociation, ionization and Coulomb explosion) according to the criteria (3.21).

In Fig. 15, we show the time-evolution of the survival, dissociation, ionization and Coulomb explosion of H_2^+ for different intensity of laser fields with wavelength λ=532nm. From Fig. 15 we can observe that the survival channel is turned off earlier with the increase of the intense laser field, simultaneously the others are turned on earlier. We can also observe that the ionization channel is turned on the earliest and the dissociation channel and the Coulomb explosion channel are turned on at the same time. Fig. 15 reveals that the probability curve of survival declines quickly, the probability curves of ionization curve and Coulomb explosion vary quite rapidly, and the dissociation curve does not vary much with respect to the intense laser field. A very interesting phenomenon is observed in Fig. 15: the probability of Coulomb explosion remains to be zero until the probability of ionization reaches its peak value, and then the probability of ionization decreases rapidly to zero. Finally, the probability of Coulomb explosion goes up rapidly and reaches its peak value and then keeps unchanged. These results are in agreement with those obtained by numerically solving the time-dependent Schrödinger equation (1D model) under the same conditions [59].

DOI https://doi.org/2007-CiCP-7894 | Generated on 2024-12-22 17:59:56
OPEN ACCESS

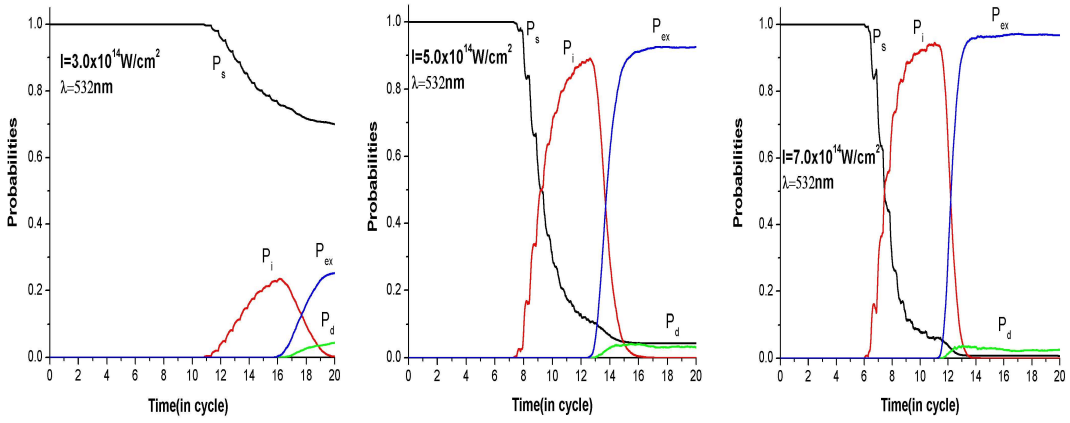

(a) (b) (c)

Figure 15: Variation of probability of survival P_s, ionization P_i, dissociation P_d and Coulomb explosion P_{ex} for different intensity of laser pulse.

4 Time-independent Schrödinger equation & symplectic-scheme shooting method

The time-independent Schrödinger equation is one of the basic equations of quantum mechanics. Its solutions are required in the studies of atomic and molecular structure and spectra, molecular dynamics and quantum chemistry. In this section, we transform the Schrödinger equation into a Hamiltonian equation by using the Legendre transformation. The resulting canonical equation is solved by symplectic methods, and techniques for solving the eigenvalues and eigenfunctions were developed [60–64].

4.1 One-dimensional time-independent Schrödinger equation

4.1.1 Symplectic form

The one-dimensional time-independent Schrödinger equation may be written in the form (atomic units are used)

$$-\frac{1}{2}\frac{d^2\psi}{dx^2}+V(x)\psi=E\psi, \tag{4.1}$$

where E is the energy eigenvalue, $V(x)$ is the potential, and $\psi(x)$ is the wave function. Eq. (4.1) can be rewritten in the form

$$\ddot{\psi}+\frac{\partial U}{\partial \psi}=0, \tag{4.2}$$

where $U(x,\psi)=\frac{1}{2}B(x)\psi^2$ and $B(x)=2[E-V(x)]$. If x is regarded as the time variable, and $\psi(x)$ and $U(x,\psi)$ are respectively regarded as a generalized coordinate and a formal potential function, then $\dot{\psi}(x)$ and $\ddot{\psi}(x)$ are the generalized velocity and the generalized

DOI https://doi.org/2007-CiCP-7894 | Generated on 2024-12-22 17:59:56
OPEN ACCESS

acceleration, respectively. Thus Eq. (4.2) is a formal Newtonian equation for a particle with a unit of mass moving in a complex functional space. In this case, if the Lagrange function,

$$L(\psi,\dot{\psi},x)=T-U=\frac{1}{2}\dot{\psi}^2-\frac{1}{2}B(x)\psi^2,$$

is regarded as a function of $\dot{\psi}$, it is a positive quadratic form in $\dot{\psi}$. The Legendre transformation of $L(\psi,\dot{\psi},x)$ is

$$H(\psi,\varphi,x)=\varphi\dot{\psi}-L(\psi,\dot{\psi},x), \tag{4.3}$$

which gives

$$\frac{\partial}{\partial\dot{\psi}}(\varphi\dot{\psi}-L(\psi,\dot{\psi},x))=0. \tag{4.4}$$

Eq. (4.4) yields $\varphi=\partial L/\partial\dot{\psi}=\dot{\psi}$. Substituting φ into Eq. (4.3), we obtain the Hamiltonian function

$$H(\psi,\varphi,x)=\frac{\varphi^2}{2}+\frac{1}{2}B(x)\psi^2. \tag{4.5}$$

Then the Hamiltonian canonical equation is

$$\begin{cases} \dot{\varphi}=-\dfrac{\partial H}{\partial\psi}=-B(x)\psi, \\ \dot{\psi}=\dfrac{\partial H}{\partial\varphi}=\varphi. \end{cases} \tag{4.6}$$

Eq. (4.6) is equivalent to the one-dimensional time-independent Schrödinger equation (4.1). The spatial variation of the solution of the canonical equation (4.6) from x_1 to x_2 is given by

$$\begin{pmatrix} \varphi(x_2) \\ \psi(x_2) \end{pmatrix}=g_H^{x_1x_2}\begin{pmatrix} \varphi(x_1) \\ \psi(x_1) \end{pmatrix}.$$

The Hamiltonian system (4.5) including explicitly the "time" variable is similar to the Hamiltonian function (2.41), and hence the explicit symplectic schemes (2.43)-(2.46) can be used to solve this system numerically.

4.1.2 Symplectic-scheme shooting method

We consider the one-dimensional eigenvalue problem with the boundary conditions

$$\psi(a)=0,\quad \psi(b)=0, \tag{4.7}$$

where a and b are, respectively, the left and right boundaries. We choose a center point $x=x_c$ ($a<x_c<b$); the calculation can be started from the left boundary to the center point ($x=x_c$) and from the right boundary to the center point ($x=x_c$), respectively. The left and right boundaries are regarded as the initial conditions.

DOI https://doi.org/2007-CiCP-7894 | Generated on 2024-12-22 17:59:56
OPEN ACCESS

We choose the following initial conditions:

$$\begin{aligned}&\text{Initial condition 1:} \quad (\varphi_L(a),\psi_L(a))=(1,0);\\ &\text{Initial condition 2:} \quad (\varphi_R(b),\psi_R(b))=(1,0),\end{aligned}$$

and obtain two solutions: `Solution 1` is $(\varphi_L(x),\psi_L(x))$, and `Solution 2` is $(\varphi_R(x),\psi_R(x))$. We know the canonical equation and the boundary conditions (4.7) are linear and homogeneous. If the initial condition is $c_1(\varphi_L(a),\psi_L(a))=c_1(1,0)$, then the corresponding solution is $c_1(\varphi_L(x),\psi_L(x))$. Likewise, the solution for the initial condition $c_2(\varphi_R(b),\psi_R(b))=c_2(1,0)$ is $c_2(\varphi_R(x),\psi_R(x))$. These two solutions must be equivalent at $x=x_c$:

$$c_1\begin{pmatrix}\varphi_L(x_c)\\ \psi_L(x_c)\end{pmatrix}=c_2\begin{pmatrix}\varphi_R(x_c)\\ \psi_R(x_c)\end{pmatrix},$$

i.e.,

$$\begin{pmatrix}\varphi_L(x_c) & -\varphi_R(x_c)\\ \psi_L(x_c) & -\psi_R(x_c)\end{pmatrix}\begin{pmatrix}c_1\\ c_2\end{pmatrix}=0. \tag{4.8}$$

The values c_1 and c_2 determined by Eq. (4.8) give the initial conditions $(c_1,0)$ and $(c_2,0)$ that we need in the computation. To obtain non-zero solutions, the determinant of the coefficient matrix of Eq. (4.8) must be zero, i.e.,

$$\det\begin{vmatrix}\varphi_L(x_c) & -\varphi_R(x_c)\\ \psi_L(x_c) & -\psi_R(x_c)\end{vmatrix}=0. \tag{4.9}$$

If we change the value of the parameter E in (4.1), then the value of the determinant of the coefficient matrix of (4.8) will be changed; the parameter E satisfying (4.9) is the eigenvalue that we need to compute. Hence (4.9) is the criterion for convergence of computation. The resulting method is called symplectic-scheme shooting method (SSSM).

We consider a Morse potential

$$V(x)=D[\exp(-2\omega x)-2\exp(-\omega x)], \tag{4.10}$$

with $D=12$ and $\omega=0.204124$ (24 bound states). The exact eigenvalues are given by

$$E_n=-12+(n+1/2)-\frac{1}{48}(n+1/2)^2, \quad n=0,1,\cdots,23. \tag{4.11}$$

We solve the eigenvalues by using the 4-stage 4th-order SSSM. The numerical eigenvalues with $a=-b=-13.5$ are given in Table 1 along with the exact ones. It shows that our results are in good agreement with the exact solutions.

4.1.3 Numerical method based on the Magnus expansion

The solution of (4.6) with the initial condition $(\varphi_0,\psi_0)^T$ is given by [65]

$$\begin{pmatrix}\varphi(x)\\ \psi(x)\end{pmatrix}=\exp(\Omega(x))\begin{pmatrix}\varphi_0\\ \psi_0\end{pmatrix}, \tag{4.12}$$

DOI https://doi.org/2007-CiCP-7894 | Generated on 2024-12-22 17:59:56
OPEN ACCESS

Table 1: Energy eigenvalues of Morse potential ($x_c=0, h=0.5\times10^{-3}$).

n	exact eigenvalue	numerical solution	n	exact eigenvalue	numerical solution
0	-11.50520833	-11.50520844	6	-6.38020833	-6.38020938
1	-10.54687500	-10.54687531	7	-5.67187500	-5.67187614
2	-9.63020833	-9.63020882	8	-5.00520833	-5.00520954
3	-8.75520833	-8.75520899	9	-4.38020833	-4.38020960
4	-7.92187500	-7.92187581	10	-3.79687500	-3.79687628
5	-7.13020833	-7.13020927	11	-3.25520833	-3.25520830

where $\Omega(x)$ is the Magnus expansion

$$\begin{aligned}\Omega(x)=&\int_0^x A(\tau)d\tau-\frac{1}{2}\int_0^x\left[\int_0^\tau A(\sigma)d\sigma,A(\tau)\right]d\tau\\&+\frac{1}{4}\int_0^x\left[\int_0^\tau\left(\int_0^\sigma A(\mu)d\mu,A(\sigma)\right)d\sigma,A(\tau)\right]d\tau\\&+\frac{1}{12}\int_0^x\left[\int_0^\tau A(\sigma)d\sigma,\left(\int_0^\tau A(\mu)d\mu,A(\tau)\right)\right]d\tau+\cdots.\end{aligned}\tag{4.13}$$

The numerical method of order two based on the Magnus expansion reads

$$\begin{pmatrix}\varphi^{n+1}\\ \psi^{n+1}\end{pmatrix}=\exp(hA(x_n+h/2))\begin{pmatrix}\varphi^n\\ \psi^n\end{pmatrix},\tag{4.14}$$

and the numerical method of order four is

$$\begin{pmatrix}\varphi^{n+1}\\ \psi^{n+1}\end{pmatrix}=\exp\left(h(A_1+A_2)/2+\sqrt{3}h^2[A_2,A_1]/12\right)\begin{pmatrix}\varphi^n\\ \psi^n\end{pmatrix},\tag{4.15}$$

where $A_1=A(x_n+c_1h)$, $A_2=A(x_n+c_2h)$, $[A_2,A_1]=A_2A_1-A_1A_2$, $c_1=1/2-\sqrt{3}/6$ and $c_2=1/2+\sqrt{3}/6$. For convenience, the matrix in the exponentials in (4.14) and (4.15) is denoted by A; hence

$$A=\begin{pmatrix}0 & -hB_{n+\frac{1}{2}}\\ h & 0\end{pmatrix}$$

for method (4.14), and

$$A=\begin{pmatrix}\frac{\sqrt{3}h^2}{12}(B_1-B_2) & -\frac{h}{2}(B_1+B_2)\\ h & -\frac{\sqrt{3}h^2}{12}(B_1-B_2)\end{pmatrix}$$

DOI https://doi.org/2007-CiCP-7894 | Generated on 2024-12-22 17:59:56
OPEN ACCESS

for method (4.15). The Taylor expansion $\exp(A)$ can be written as $\exp(A)=I+A+\frac{1}{2!}A^2+\frac{1}{3!}A^3+\frac{1}{4!}A^4+\cdots$. In the following discussion, we take the method (4.14) as an example; and take for convenience $B=B_{n+1/2}=B(x_n+h/2)$. Thus

$$\begin{aligned}\exp(A)=&I+\begin{pmatrix}0&-hB\\h&0\end{pmatrix}+\frac{1}{2!}\begin{pmatrix}-h^2B&0\\0&-h^2B\end{pmatrix}+\frac{1}{3!}\begin{pmatrix}0&h^3B^2\\-h^3B&0\end{pmatrix}\\&+\cdots+\frac{1}{(2k)!}\begin{pmatrix}(-1)^kh^{2k}B^k&0\\0&(-1)^kh^{2k}B^k\end{pmatrix}\\&+\frac{1}{(2k+1)!}\begin{pmatrix}0&(-1)^{k+1}h^{2k+1}B^{k+1}\\(-1)^kh^{2k+1}B^k&0\end{pmatrix}+\cdots.\end{aligned}$$

Then we can obtain the following matrix:

$$\exp(A)=\begin{bmatrix}\displaystyle\sum_{k=0}\frac{1}{(2k)!}(-1)^kh^{2k}B^k&\displaystyle\sum_{k=0}\frac{1}{(2k+1)!}(-1)^{k+1}h^{2k+1}B^{k+1}\\\displaystyle\sum_{k=0}\frac{1}{(2k+1)!}(-1)^kh^{2k+1}B^k&\displaystyle\sum_{k=0}\frac{1}{(2k)!}(-1)^kh^{2k}B^k\end{bmatrix}.\tag{4.16}$$

Considering the $2p$-th order approximation of the Taylor expansion for $\exp(A)$ ($n=2p$),

$$\begin{aligned}\exp(A)=&\begin{pmatrix}\displaystyle\sum_{k=0}^{p}\frac{1}{(2k)!}(-1)^kh^{2k}B_{n+\frac12}^k&\displaystyle\sum_{k=0}^{p-1}\frac{1}{(2k+1)!}(-1)^{k+1}h^{2k+1}B_{n+\frac12}^{k+1}\\\displaystyle\sum_{k=0}^{p-1}\frac{1}{(2k+1)!}(-1)^kh^{2k+1}B_{n+\frac12}^k&\displaystyle\sum_{k=0}^{p}\frac{1}{(2k)!}(-1)^kh^{2k}B_{n+\frac12}^k\end{pmatrix}\\=:&\begin{pmatrix}M_{11}^n&M_{12}^n\\M_{21}^n&M_{22}^n\end{pmatrix},\end{aligned}$$

we obtain

$$\begin{pmatrix}\varphi^{n+1}\\\psi^{n+1}\end{pmatrix}=\exp(A)\begin{pmatrix}\varphi^n\\\psi^n\end{pmatrix}=\begin{pmatrix}M_{11}^n&M_{12}^n\\M_{21}^n&M_{22}^n\end{pmatrix}\begin{pmatrix}\varphi^n\\\psi^n\end{pmatrix}.\tag{4.17}$$

Eliminating φ^n and φ^{n+1}, we have

$$M_{21}^{n-1}\psi^{n+1}-(M_{21}^{n-1}M_{22}^n+M_{21}^nM_{11}^{n-1})\psi^n+M_{21}^n(M_{11}^{n-1}M_{22}^{n-1}-M_{21}^{n-1}M_{12}^{n-1})\psi^{n-1}=0,\tag{4.18}$$

which is a generalized matrix eigenvalue equation. Eq. (4.18) can be written as $C_1\psi^{n+1}-C_2\psi^n+C_3\psi^{n-1}=0$, or equivalently,

$$\psi^{n+1}=C_1^{-1}(C_2\psi^n-C_3\psi^{n-1}),\tag{4.19}$$

which is a three-layer scheme, where C_1, C_2 and C_3 can be determined by (4.18).

Now we consider the one-dimensional eigenvalue problem with boundary conditions (4.7) [66]. If we have the values of ψ^0 and ψ^1, the equation can be solved easily using the

DOI https://doi.org/2007-CiCP-7894 | Generated on 2024-12-22 17:59:56
OPEN ACCESS

Table 2: The eigenvalues for the harmonic oscillator. $a=-15.5$, $b=15.5$, space step $h=10^{-4}$.

n	exact eigenvalue	numerical solution	n	exact eigenvalue	numerical solution
0	0.50	0.50000000169	4	4.50	4.50000000026
1	1.50	1.49999999967	5	5.50	5.49999999946
2	2.50	2.50000000056	6	6.50	6.50000000031
3	3.50	3.50000000122			

schemes (4.19). We know the left boundary condition $\psi^0=\psi(a)=0$, and we set $\psi^1=$ const.$\neq 0$. Thus, the solutions $(\psi^0,\psi^1,\cdots,\psi^N)$ can be obtained by using the scheme (4.19). In the calculation, we may take $\psi^1=1$. The solutions are independent of ψ^1 if $\psi^1\neq 0$ due to the fact that $\psi^0=0$. Because of the right boundary condition, $\psi^N=\psi(b)=0$, we must find the value of the parameter E that makes $\psi^N=0$. Note that the coefficients C_1,C_2 and C_3 are functions of the parameter E. If we change the values of E, we obtain a series for ψ_E^N. According to the right boundary condition $\psi^N=0$, the parameter E that makes $\psi_E^N=0$ is the eigenvalue that we need to compute.

The potential of the one-dimensional harmonic oscillator is taken to be $V(x)=x^2/2$, $x\in\mathbb{R}$. The exact eigenvalues of the harmonic oscillator are given by $E_n=n+1/2$, $n=0,1,\cdots$. The eigenvalues obtained by using the shooting method that uses schemes of 4th-order approximation with the Taylor expansion of the matrix exponential are listed in Table 2, which are compared with the exact ones. Again, it is observed that the numerical results are in good agreement with the exact ones.

4.2 Continuum eigenfunction of the Schrödinger equation

It may be assumed that the potential $V(x)$ in the 1D time-independent Schrödinger equation (4.1) is an even function. For example, the Pöschl-Teller short-range potential $V(x)=-U_0/\cosh^2(\alpha_0 x)$ is an even function. It indicates that in quantum mechanics the continuous spectrum is doubly degenerate when $E>0$, that is to say, for each desired value of $E>0$, the 1D time-independent Schrödinger equation (4.1) possesses two linearly independent continuum eigen-functions (LICEF), and they may be chosen as the even parity $\psi_e(x)$ (even eigen-function) and odd parity (odd eigen-function) $\psi_o(x)$, respectively. Let $\varphi_e(x)=\dot{\psi}_e(x)$ and $\varphi_o(x)=\dot{\psi}_o(x)$. Then the necessary and sufficient condition for $\psi_e(x)$ and $\psi_o(x)$ to be linearly independent is the Wronskian conservation, namely,

$$\begin{vmatrix} \psi_e(x) & \varphi_e(x) \\ \psi_o(x) & \varphi_o(x) \end{vmatrix} = \text{const.} \neq 0.$$

Hence a Wronskian-preserving algorithm should be adopted for the computation of LICEF. For each spatial point x, $(\psi_e(x),\varphi_e(x))^T$ and $(\psi_o(x),\varphi_o(x))^T$ are both two-dimensional

DOI https://doi.org/2007-CiCP-7894 | Generated on 2024-12-22 17:59:56
OPEN ACCESS

Table 3: Wronskian of two linearly independent solutions of the Pöschl-Teller short-range potential ($U_0=0.7,\alpha_0=0.4$) for $h=0.1$ and $E=0.01a.u.$

x	Explicit RK	Explicit symplectic	Exact values
0.0	1.0000000000	1.0000000000	1.0000000000
1.0	0.9999996362	1.0000000000	1.0000000000
2.0	0.9999994712	1.0000000000	1.0000000000
3.0	0.9999994303	1.0000000000	1.0000000000
4.0	0.9999994230	1.0000000000	1.0000000000
5.0	0.9999994218	1.0000000000	1.0000000000

vectors, their symplectic product is

$$\begin{aligned}&[(\psi_e(x),\varphi_e(x))^T,(\psi_o(x),\varphi_o(x))^T]\\&=(\psi_e(x),\varphi_e(x))\begin{pmatrix}0&1\\-1&0\end{pmatrix}\begin{pmatrix}\psi_o(x)\\\varphi_o(x)\end{pmatrix}=\begin{vmatrix}\psi_e(x)&\varphi_e(x)\\\psi_o(x)&\varphi_o(x)\end{vmatrix},\end{aligned}\tag{4.20}$$

which is just the Wronskian of ψ_e and ψ_o, see, e.g., [67–69].

From the above analysis, for each desired eigen-energy $E>0$ it can be assumed that the two LICEF are $\psi_e(x)$ and $\psi_o(x)$, respectively. We only need to solve the canonical equation (4.6) with the initial values

$$(\psi_e(0),\dot{\psi}_e(0))=(1,0)\quad\text{and}\quad(\psi_o(0),\dot{\psi}_o(0))=(0,1),\tag{4.21}$$

in $[0,\infty)$, using the symplectic algorithm. We calculate the CEF $\psi_e(x)$ and $\psi_o(x)$ of the 1-D Pöschl-Teller short-range potential for $E=0.01a.u.$ and $h=0.1$ and $R=500a.u.$, and the numerical results are represented Fig. 16. In order to compare the results obtained by the explicit symplectic algorithm with the ones by the explicit RK method, we list some numerical values of Wronskian in Table 3. From this table, it can be seen that the numerical values obtained by the explicit symplectic algorithm are almost equal to the exact values, in contrast to those by the explicit RK method.

4.3 Two-dimensional time-independent Schrödinger equation

4.3.1 Symplectic and multi-symplectic form

In atomic units, the two-dimensional time-independent Schrödinger equation may be written in the form

$$-\frac{1}{2}\frac{\partial^2\psi}{\partial x^2}-\frac{1}{2}\frac{\partial^2\psi}{\partial y^2}+V(x,y)\psi=E\psi,\tag{4.22}$$

$$\psi(x,\pm\infty)=0,\quad-\infty<x<+\infty,\tag{4.23}$$

$$\psi(\pm\infty,y)=0,\quad-\infty<y<+\infty,\tag{4.24}$$

DOI https://doi.org/2007-CiCP-7894 | Generated on 2024-12-22 17:59:56
OPEN ACCESS

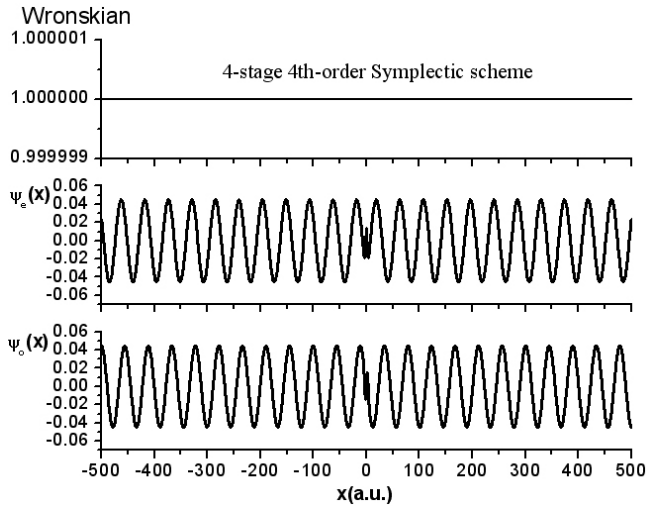

Figure 16: Even parity and odd parity CEF of Pöschl-Teller short-range potential.

where E is the energy eigenvalue, $V(x,y)$ the potential, and $\psi(x,y)$ the wave function. Substituting the symmetry difference quotient for the partial derivative $\partial^2\psi/\partial y^2$, and considering the boundary conditions (4.23), we obtain, for $-N+1\leq j\leq N-1$,

$$\frac{\partial^2\psi(x,y_j)}{\partial x^2}=-\frac{1}{\Delta y^2}\psi(x,y_{j-1})-B(x,y_j)\psi(x,y_j)-\frac{1}{\Delta y^2}\psi(x,y_{j+1}), \tag{4.25}$$

where $B(x,y_j)=2[E-V(x,y_j)-1/\Delta y^2]$. If we let

$$\psi=[\psi(x,y_{-N+1}),\cdots,\psi(x,y_{N-1})]^T,\quad \varphi=\dot{\psi}=[\dot{\psi}(x,y_{-N+1}),\cdots,\dot{\psi}(x,y_{N-1})]^T, \tag{4.26}$$

then Eq. (4.25) can be rewritten in matrix form as [70]

$$\dot{\varphi}=-S\psi,\quad \dot{\psi}=\varphi, \tag{4.27}$$

where the upper dot denotes the derivative with respect to x, $S(x)$ is a $(2N-1)$-order tridiagonal symmetric matrix, $S^T=S$. Eq. (4.27) is the Hamiltonian canonical equation, and its Hamiltonian function is

$$H=\frac{1}{2}z^TCz=\frac{1}{2}\varphi^T\varphi+\frac{1}{2}\psi^TS\psi. \tag{4.28}$$

Set $v_x+w_y+N'(\psi)=0$, $v=\psi_x+p_y$, $w=\psi_y-p_x$, $w_x-v_y=0$, and $N(\psi)=[V(x,y)-E]\psi^2$. Then the two-dimensional time-independent Schrödinger equation can be reformulated in the multisymplectic Hamiltonian form

$$M\frac{\partial z}{\partial x}+K\frac{\partial z}{\partial y}=\nabla_z S(z),$$

DOI https://doi.org/2007-CiCP-7894 | Generated on 2024-12-22 17:59:56
OPEN ACCESS

Table 4: Eigenvalues of the two-dimensional harmonic oscillator.

	Method2	Method3	Exact		Method2	Method3	Exact
$E0$	1.000625	1.000104	1	$E7$	7.980570	8.000187	8
$E1$	1.999373	2.000102	2	$E8$	8.975551	9.000005	9
$E2$	2.998121	3.000100	3	$E9$	9.969271	10.000005	10
$E3$	3.995616	4.000096	4	$E10$	10.962991	11.000152	11
$E4$	4.993111	5.000098	5	$E11$	11.955448	12.000899	12
$E5$	5.989352	6.000068	6	$E12$	12.947904	12.999864	13
$E6$	6.985589	6.999995	7				

where

$$M=\begin{bmatrix} 0 & -1 & 0 & 0 \\ 1 & 0 & 0 & 0 \\ 0 & 0 & 0 & -1 \\ 0 & 0 & 1 & 0 \end{bmatrix}, \quad K=\begin{bmatrix} 0 & 0 & -1 & 0 \\ 0 & 0 & 0 & 1 \\ 1 & 0 & 0 & 0 \\ 0 & -1 & 0 & 0 \end{bmatrix}, \quad z=\begin{pmatrix} \psi \\ v \\ w \\ p \end{pmatrix},$$

and $S(z)=(v^2+w^2)/2+N(\psi)$. There are two symplectic structures, i.e.

$$\omega_1=dv\wedge d\psi+dp\wedge dw, \quad \omega_2=dw\wedge d\psi+dv\wedge dp$$

and a multisymplectic scheme can be used to solve the Schrödinger equation [24,25].

4.3.2 Two-dimensional eigenvalue problem

The one-dimensional SSSM can be easily extended to the calculations of the two-dimensional eigenvalue problem. We can find the computational details from our previous work [61,70].

Recently, Simos and his collaborators [71–76] improved the numerical method for solving the time-independent Schrödinger equation by using symplectic method. Monovasilis et al. [76] improved the symplectic scheme-matrix eigenvalue method (SSMEM) for the numerical solution of the two-dimensional time independent Schrödinger equation and presented a numerical method by third-order symplectic schemes. In their work, the eigenvalue problem is transformed into an algebraic eigenvalue problem involving real, symmetric, large sparse matrices. The application of the third-order symplectic method to the two-dimensional eigenvalue problem gave an algebraic eigenvalue problem

$$(P+Eh^2Q+E^2h^4R+E^3h^6S+E^4h^8F-E^5h^{10}Z)\Psi=0, \tag{4.29}$$

where the coefficients P, Q, R, S, F, Z can be found in [76].

The potential of the two-dimensional harmonic oscillator is taken to be $V(x,y)=(x^2+y^2)/2$. The exact eigenvalues of the two-dimensional harmonic oscillator are given by $E_n=n+1, n=n_x+n_y, (n_x,n_y=0,1,\cdots)$. The eigenvalues of the two-dimensional harmonic oscillator obtained from method (4.29) are listed in Table 4, which is from [76]. We see

DOI https://doi.org/2007-CiCP-7894 | Generated on 2024-12-22 17:59:56
OPEN ACCESS

that the 3rd-order symplectic method (Method 3) gives better results than the second-order symplectic method (Method 2). It shows that the higher-order symplectic method can produce more accurate results.

5 Interaction of atoms with intense laser field and the time-dependent Schrödinger equation

With the development of laser techniques, laser-atom interaction has become one of the very interesting topics [77,78]. In recent years, a number of experiments on intense laser pulses probing laser-atom interaction have produced many new results, such as multi-photon ionization (MPI) rates, above-threshold ionization (ATI) and high-order harmonic generation (HHG). The high-order harmonics up to the order 300 (with the maximum energy about 0.5keV) have been observed in recent experiments in helium atom [79], which has been in the "water windows" range. Many theoretical works have been developed in understanding laser-atom interaction. We give the asymptotic boundary conditions for solving the time-dependent Schrödinger equation of atom in an intense laser field, and study the behaviors and high-order harmonic generation for atoms in the intense laser field in this section.

5.1 Mathematical model and asymptotic boundary condition

In the length gauge, the one-dimensional time-dependent Schrödinger equation of an atom in a laser field reads (in atomic units)

$$i\frac{\partial}{\partial t}\psi(x,t)=\left[-\frac{1}{2}\frac{\partial^2}{\partial x^2}+V(x)-\varepsilon(t)x\right]\psi(x,t),\quad t>0,x\in\mathbb{R}, \tag{5.1}$$

where $V(x)$ is the short-range model potential. We add the laser-atom interaction in the dipole approximation

$$\varepsilon(t)x=\varepsilon_0 f(t)\cos(\omega_0 t)x,$$

where ε_0 is the peak intensity of the laser field, $f(t)$ is the function that describes the temporal shape of the pulse, with the light assumed to be linearly polarized, and $f(t)=\sin^2(\Omega t)$. The initial condition is set to be the ground state wavefunction $\varphi(x)$.

Since the potential $V(x)$ is short-range, it has monotonous attenuation with increasing of $|x|$. If we omit the effect of the short-range potential in the sufficiently large distance, Eq. (5.1) becomes

$$i\frac{\partial}{\partial t}\psi(x,t)=\left[-\frac{1}{2}\frac{\partial^2}{\partial x^2}-\varepsilon(t)x\right]\psi(x,t),\quad t>0,x\in\mathbb{R}. \tag{5.2}$$

Eq. (5.2) can be solved by Fourier transformation methods [80,81]. Considering the phase integral method [82], we can obtain the solution of Eq. (5.2) at $x=\pm X_0$:

$$\psi(\pm X_0,t)=\exp(-iA(\pm X_0)-iq/2)\varphi(\pm X_0-\alpha), \tag{5.3}$$

DOI https://doi.org/2007-CiCP-7894 | Generated on 2024-12-22 17:59:56
OPEN ACCESS

where $X_0>0$ is a sufficiently large parameter, $A(t)=-\int_0^t \varepsilon(t')dt'$ is the vector potential, $\alpha(t)=-\int_0^t A(t')dt'$ and $q(t)=\int_0^t A^2(t')dt'$. We call Eq. (5.3) the asymptotic boundary conditions for solving the Schrödinger equation (5.1).

5.2 Symplectic discretization based on asymptotic boundary conditions

Let $\psi(x,t)=q(x,t)+ip(x,t)$ and $U(x,t)=V(x)-\varepsilon(t)x$. The interval $(-X_0,X_0)$ can be divided into $2N$ equal segments, and the length of each segment is $h=X_0/N$. By using the asymptotic boundary condition (5.3), and substituting the symmetry difference quotient for the partial derivative, Eq. (5.1) can be discretized into the $(2N-1)$-dimensional Hamiltonian canonical equation [80, 81],

$$\dot{P}=-SQ+Y_2, \quad \dot{Q}=SP-Y_1, \tag{5.4}$$

where P and Q are two column vectors formed with values of different space nodes, $Y_1=(2h^2)^{-1}(p_{-N},0,\cdots,0,p_N)^T$, $Y_2=(2h^2)^{-1}(q_{-N},0,\cdots,0,q_N)^T$, and S is a tridiagonal-symmetric matrix [80]. The Hamiltonian function of the canonical equation (5.4) is

$$H(P,Q,t)=\frac{1}{2}P^TSP+Y_2^TP+\frac{1}{2}Q^TSQ+Y_1^TQ=H_1(P,t)+H_2(Q,t). \tag{5.5}$$

The Hamiltonian system contains explicitly the time variable, which is similar to system (2.38); thus, an explicit symplectic scheme can be used to solve it. This discretization method is called the symplectic discretization based on the asymptotic boundary condition.

5.3 Symplectic discretization based on the eigenfunction expansion

Another approach to the solution of Eq. (5.1) is to expand $\psi(x,t)$ in terms of the bound eigenfunctions φ_j and the continuum eigenfunctions ϕ_ε:

$$\psi(x,t)=\sum_j (a_j(t)+ib_j(t))\varphi_j+\int_{-\infty}^{\infty}(c_\varepsilon(t)+id_\varepsilon(t))\phi_\varepsilon d\varepsilon, \tag{5.6}$$

where φ_j and ϕ_ε can be obtained by the method presented in Section 4. Here j denotes the sum for all the bound states, ε denotes the integration over all the continuum states. The two bound states satisfy the relation $\int_{-\infty}^{\infty}\varphi_i(x)\varphi_j(x)=\delta_{ij}$, and the two continuum states in the meaning of the δ-function satisfy the relation

$$\int_{\triangle}d\varepsilon\int_{-\infty}^{\infty}\phi_{\varepsilon'}(x)\phi_\varepsilon(x)dx=\begin{cases}0 & \varepsilon' \text{ outside } \triangle,\\ 1 & \varepsilon' \text{ inside } \triangle.\end{cases}$$

They also satisfy the orthogonality relation $\int_{-\infty}^{\infty}\varphi_i\phi_\varepsilon dx=0$. The expansion coefficients can be found by mocking up the continuum by means of a set of pseudo-discrete spectra, thereby converting the mixed discrete-continuum problem into what is formally a

DOI https://doi.org/2007-CiCP-7894 | Generated on 2024-12-22 17:59:56
OPEN ACCESS

purely discrete problem [83]. In order to mock up the continuum as a set of discrete states we first divide the desired energy range $[0,E_{\max}]$ of the continuum up into different segments. If $[0,E_{\max}]$ is divided into $[0,\varepsilon_1],\cdots[\varepsilon_{i-1},\varepsilon_i],\cdots,[\varepsilon_{k-1},E_{\max}]$ and the i^{th} energy segment is Δ_i, with $\sum_{i=1}^{k}\Delta_i=E_M$, then the value of Δ_i must be chosen as a compromise between the adequate resolution of continuum detail and the limitation on the computation in order to decrease the use of the computer RAM and the CPU time. If the i^{th} pseudo-discrete energy is ε_i and its corresponding eigenfunction is ϕ_{ε_i}, then the formulation (5.6) transforms to

$$\psi(x,t)=\sum_j(a_j(t)+ib_j(t))\varphi_j+\sum_{i=1}^{k}\Delta_i(c_{\varepsilon_i}(t)+id_{\varepsilon_i}(t))\phi_{\varepsilon_i}. \tag{5.7}$$

Let $\tilde{c}_{\varepsilon_i}(t)=\sqrt{\Delta_i}c_{\varepsilon_i}(t)$, $\tilde{d}_{\varepsilon_i}(t)=\sqrt{\Delta_i}d_{\varepsilon_i}(t)$, $\tilde{\phi}_{\varepsilon_i}=\sqrt{\Delta_i}\phi_{\varepsilon_i}$. Thus the formula (5.7) can be rewritten as

$$\psi(x,t)=\sum_j(a_j(t)+ib_j(t))\varphi_j+\sum_{l=1}^{k}(\tilde{c}_{\varepsilon_l}(t)+i\tilde{d}_{\varepsilon_l}(t))\tilde{\phi}_{\varepsilon_l}. \tag{5.8}$$

Inserting (5.8) into (5.1) and integrating the resulting equation over φ_l, where φ_l is ergodic including all of the discrete states and the pseudo-discrete states, yield

$$\begin{cases}\dot{a}_l=\Big[E_lb_l+\sum_j b_j<\varphi_l|V|\varphi_j>+\sum_{i=1}^{k}\tilde{d}_{\varepsilon_i}<\varphi_l|V|\tilde{\phi}_{\varepsilon_i}>\Big],\\ \dot{\tilde{c}}_{\varepsilon_l}=\Big[\varepsilon_l\tilde{d}_{\varepsilon_l}+\sum_j b_j<\tilde{\phi}_{\varepsilon_l}|V|\varphi_j>+\sum_{i=1}^{k}\tilde{d}_{\varepsilon_i}<\tilde{\phi}_{\varepsilon_l}|V|\tilde{\phi}_{\varepsilon_i}>\Big],\\ \dot{b}_l=-\Big[E_la_l+\sum_j a_j<\varphi_l|V|\varphi_j>+\sum_{i=1}^{k}\tilde{c}_{\varepsilon_l}<\varphi_l|V|\tilde{\phi}_{\varepsilon_i}>\Big],\\ \dot{\tilde{d}}_{\varepsilon_l}=-\Big[\varepsilon_l\tilde{c}_{\varepsilon_l}+\sum_j a_j<\tilde{\phi}_{\varepsilon_l}|V|\varphi_j>+\sum_{i=1}^{k}\tilde{c}_{\varepsilon_l}<\tilde{\phi}_{\varepsilon_l}|V|\tilde{\phi}_{\varepsilon_i}>\Big].\end{cases} \tag{5.9}$$

Let

$$A=\left(\underbrace{a_1,\cdots,a_{n_d}}_{discrete},\underbrace{\tilde{c}_{\varepsilon_1},\cdots,\tilde{c}_{\varepsilon_{n_c}}}_{continuum}\right)^T,\quad B=\left(\underbrace{b_1,\cdots,b_{n_d}}_{discrete},\underbrace{\tilde{d}_{\varepsilon_1},\cdots,\tilde{d}_{\varepsilon_{n_c}}}_{continuum}\right)^T,$$

$E_D=[E_l]$ be the discrete eigenmatrix, $E_C=[\varepsilon_i]$ be the pseudo-discrete eigenmatrix, $V_{DD}=[<\varphi_l|V|\varphi_j>]$ be the matrix between the discrete states, $V_{DC}=[<\varphi_l|V|\tilde{\phi}_{\varepsilon_i}>]$ be the matrix between the discrete states and the pseudo-discrete states, $V_{CD}=[<\tilde{\phi}_{\varepsilon_i}|V|\varphi_j>]$ be the matrix between the pseudo-discrete states and the discrete states, and $V_{CC}=[<\tilde{\phi}_{\varepsilon_i}|V|\tilde{\phi}_{\varepsilon_i}>]$ be the matrix between the pseudo-discrete states, where n_d and n_c are the numbers of the discrete states and the pseudo-discrete states, respectively. We have $V_{DC}=(V_{CD})^T$.

DOI https://doi.org/2007-CiCP-7894 | Generated on 2024-12-22 17:59:56
OPEN ACCESS

Inserting these quantities into (5.9), we obtain the Hamiltonian equation

$$\dot{A}=\begin{bmatrix} E_D+V_{DD} & V_{DC} \\ (V_{DC})^T & E_C+V_{CC} \end{bmatrix} B, \quad \dot{B}=-\begin{bmatrix} E_D+V_{DD} & V_{DC} \\ (V_{DC})^T & E_C+V_{CC} \end{bmatrix} A, \tag{5.10}$$

whose Hamiltonian function is

$$\begin{aligned} H(A,B,t)&=\frac{1}{2}Z^TCZ=\frac{1}{2}\left(A^T,B^T\right)\begin{pmatrix} S & 0 \\ 0 & S \end{pmatrix}\begin{pmatrix} A \\ B \end{pmatrix} \\ &=\frac{1}{2}A^TSA+\frac{1}{2}B^TSB=H_2(A,t)+H_1(B,t). \end{aligned} \tag{5.11}$$

The system (5.11) is a Hamiltonian system containing explicitly the time variable, which is similar to system (2.38). Thus an explicit symplectic scheme can be used to solve it.

This discretization method is called the pseudo-discrete approximation or pseudo-spectrum expansion based on the numerical eigenfunction.

5.4 Harmonic generation for atoms in intense laser field

5.4.1 The Pöschl-Teller potential

The 1-D Pöschl-Teller (P-T) short-range potential can be written as

$$V_0(x)=-U_0/\cosh^2(\alpha_0 x), \tag{5.12}$$

which possesses the following properties:

1. $V_0(x)$ is an even function, namely, $V_0(-x)=V_0(x)$;
2. $|V_0(x)|$ falls off exponentially as $|x|$ increases;
3. There is a finite number of bound levels for given parameters U_0 and α_0.

5.4.2 Hydrogen atom (H) and Helium ion (H_e^+)

When the atom moves in the linear-polarized laser field, the soft-core potential

$$V_0(x)=-Z/\sqrt{x^2+\alpha^2} \tag{5.13}$$

is adopted, where α and Z are introduced to remove the singularity at the origin and to adjust the depth of the potential well. We point out that most properties of a real atom can be reproduced by adjusting the parameters α and z, for example, $\alpha=\sqrt{2}$, $Z=1$ for the 1-D H atom, and $\alpha=0.5$, $Z=2$ for the 1-D H_e^+. The potential (5.13) possesses the following properties:

1. $V_0(x)$ is an even function;
2. $V_0(x)\approx 1/|x|$ for sufficiently large $|x|$; this will ensure the Coulomb behavior near and above the ionization threshold;
3. $|V_0(x)|$ falls off monotonously and trends to zero with increasing $|x|$.

DOI https://doi.org/2007-CiCP-7894 | Generated on 2024-12-22 17:59:56
OPEN ACCESS

5.4.3 High-order harmonic generation for 1-D H_e^+ in the two-color laser field

The high-order harmonic of the 1-D H_e^+ in the intense two-color laser field was illustrated by the numerical method based on the asymptotic boundary condition. Fig. 17(a) shows that the 1-D H_e^+ in the laser field for the intensity $E_0 = 0.336 a.u.$ and the pulse $T = 5fs$ can generate up to 500th-order harmonic but the conversion efficiency of the harmonic is very low. It has been demonstrated theoretically and experimentally that an intense two-color laser pulse can be used to enhance the harmonic efficiency [84].

Figs. 17(b)-(d) show that the harmonics of 1-D H_e^+ subject to the two-color laser pulse are enhanced. To analyze the reason, we calculated the population of the ground state and the first excited state of 1-D H_e^+ subject to the two-color laser field. From Fig. 18 and Fig. 19, we can see that the population of the ground state has a significant decrease and the population of the first excited state has a significant increase when the two-color laser pulses with the high frequency were used. These phenomena can be explained as follows: the ionization is enhanced and the channel of the transition to the even continuum state is more unobstructed when the atom is subjected to the two-color laser pulse, as reported in [85].

5.4.4 Multi-photon ionization, above-threshold ionization, Rabi oscillation and oscillation excitation of 1-D model atom in the intense laser field

A. Ionization behavior for the P-T potential with one bound state

For $U_0 = 1$ and $\alpha_0 = 1$, there is only one bound state with eigenenergy $E_0 = -0.5 a.u.$ for the P-T potential (5.12), and the corresponding normalized eigenfunction $\varphi_o(x) = 1/(\sqrt{2}\cosh x)$, which is chosen as the initial input. The laser field $\varepsilon(t)x = \varepsilon_0 x \sin(\omega_0 t)$ is linear polarized.

Fig. 20 shows the evolution of the normalization of the wave function in the range $[-50 a.u., 50 a.u.]$ for laser intensity $\varepsilon_0 = 0.1 a.u.$, the boundary is chosen as $600 a.u.$, and the time is after 16 optical periods pulse. In this calculation, we choose the frequency $\omega_0 = 0.2 a.u.$. Fig. 20(a) is identical to Fig. 2 of [85], which shows that the ABC presented is reasonable for the interaction between the laser and the atom. The difference of the absolute value of the wave functions between the boundaries imposed on $600 a.u.$ and $700 a.u.$ is shown in Fig. 20(b), whose maximum is within the numerical computing error 10^{-4}. In Fig. 20(c), the normalization of the wave function is greater than 1 at a few points but does not exceed 10^{-11}, which is far less than the numerical error 10^{-4}, and less than 1 at most points. This result shows that there are some probabilities for electrons to be ionized into the free electron and they cannot be recombined to the parent atom.

The ionization probability of the electron is computed for the P-T potential in the laser field. The results are given in Fig. 21. The probability density of the electronic wave function

$$P(x,T) = |\psi(x,T)|^2$$

is evaluated and shown in Fig. 22. The ionization curve in Fig. 21 is identical to Fig. 6 of [84] and Fig. 3 of [85], which further shows that the ABC presented in this paper is

DOI https://doi.org/2007-CiCP-7894 | Generated on 2024-12-22 17:59:56
OPEN ACCESS

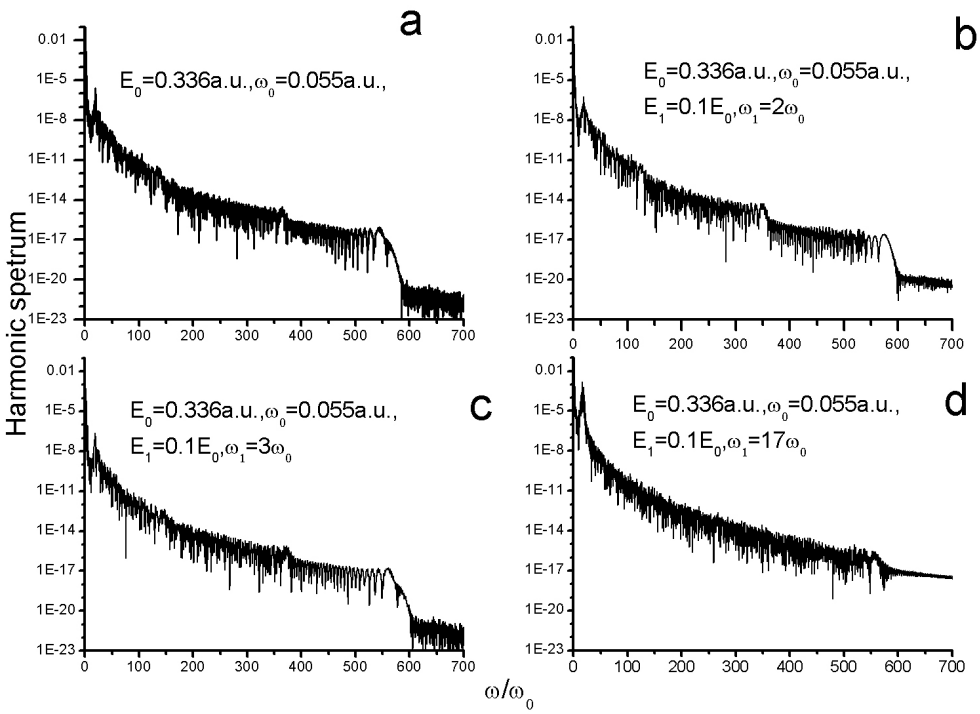

Figure 17: Harmonic spectrum irradiated by the different laser field parameter.

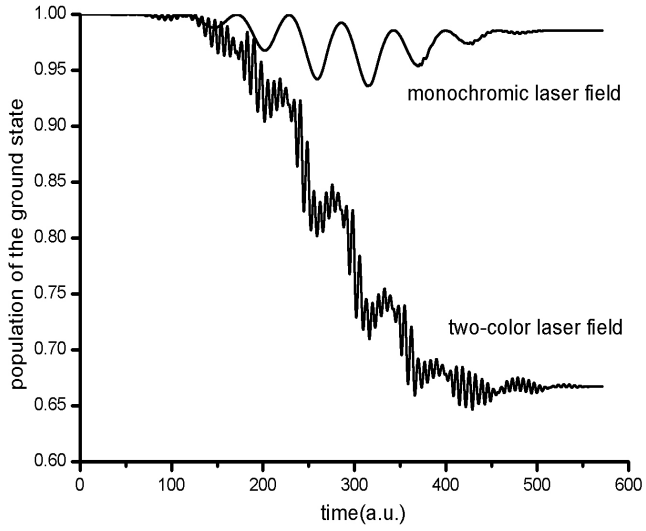

Figure 18: Probabilities of H_e^+ ground state irradiated by both of monochromic laser field ($\omega_0 = 0.055 a.u.$) and two-color ($17\omega_0$) laser field.

DOI https://doi.org/2007-CiCP-7894 | Generated on 2024-12-22 17:59:56
OPEN ACCESS

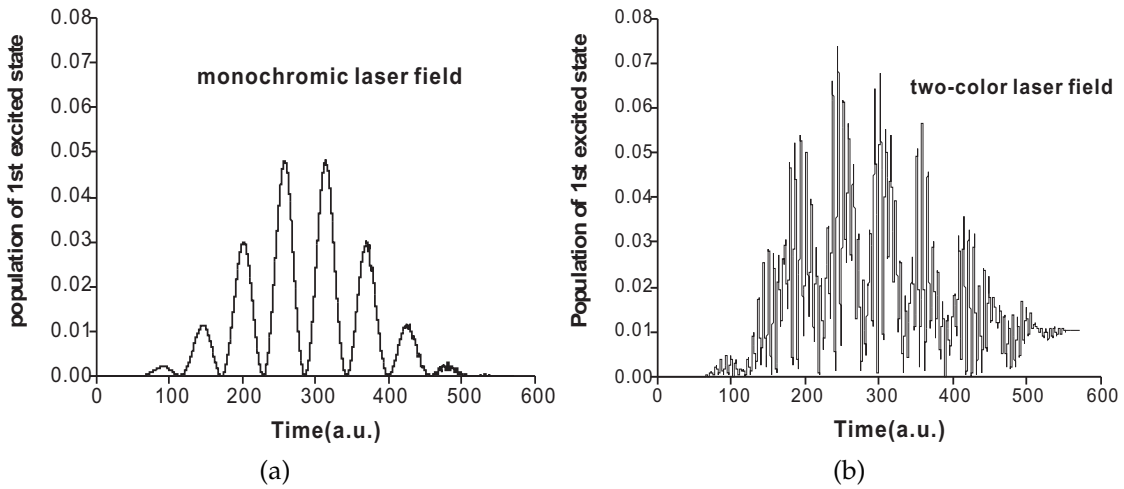

Figure 19: (a) Probabilities of H_e^+ first excited state irradiated by the monochromic laser field $\omega_0 = 0.055 a.u.$; (b) probabilities of H_e^+ first excited state irradiated by the two-color laser field $\omega_1 = 17\omega_0$.

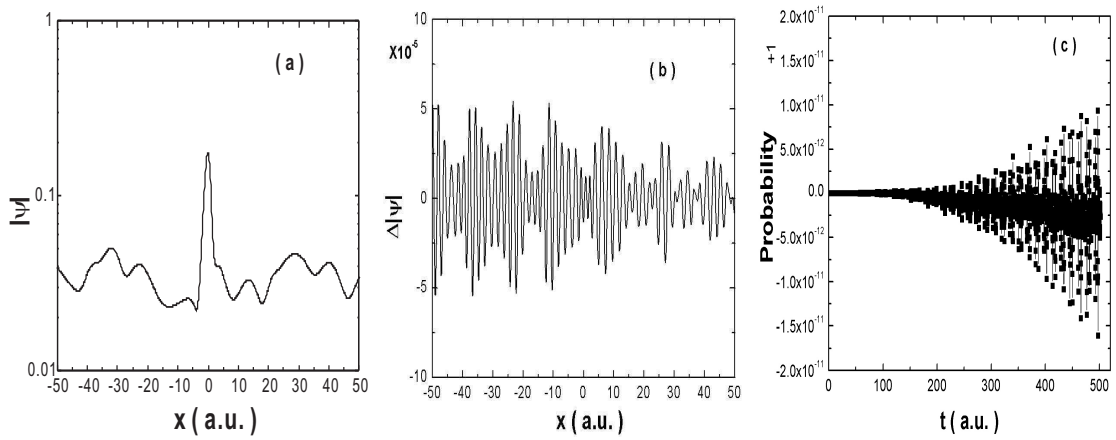

Figure 20: (a) Numerical solution $|\psi(x)|$ after 16 light periods for $\varepsilon_0 = 0.1 a.u.$ and $\omega_0 = 0.2 a.u.$; (b) Relative difference in units of 10^{-5} between the truncated solutions with boundaries at $x = \pm 600 a.u.$ and $x = \pm 700 a.u.$; (c) The normalization of wave function for $x = \pm 700 a.u.$.

reasonable and the symplectic algorithm is stable for the interaction between the laser and atom. The extrema points on the ionization curves correspond to the suppression of 3-photon ionization (A) and 4-photon ionization (B), respectively, the reason being that when

$$n\omega_0 < |E_0| + U_p, \qquad U_p = \varepsilon_0^2 / 4\omega_0^2,$$

n-photon ionization is suppressed. Furthermore, it is seen that the ionization curves are similar for different pulse width, but the ionization amplitude is different. The longer the laser pulse width, the larger the ionization amplitude. It is observed from Fig. 22 that the

DOI https://doi.org/2007-CiCP-7894 | Generated on 2024-12-22 17:59:56
OPEN ACCESS

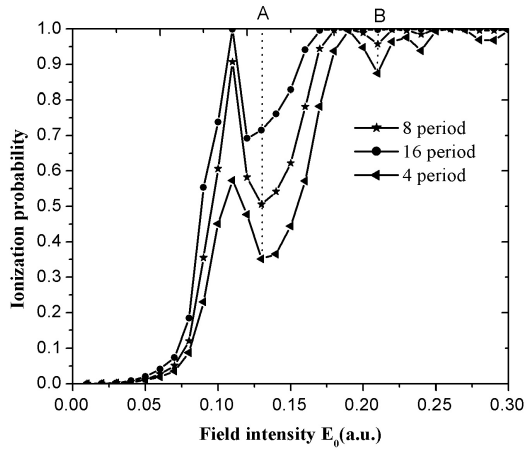

Figure 21: The ionization probability with the laser peak intensity after four (◀), eight (★) and sixteen (●) light periods for the monochromatic with frequency $\omega_0 = 0.2a.u.$.

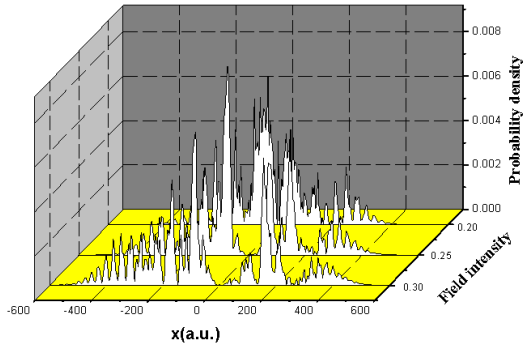

Figure 22: Probability density of wave function with the peak value of the laser intensity

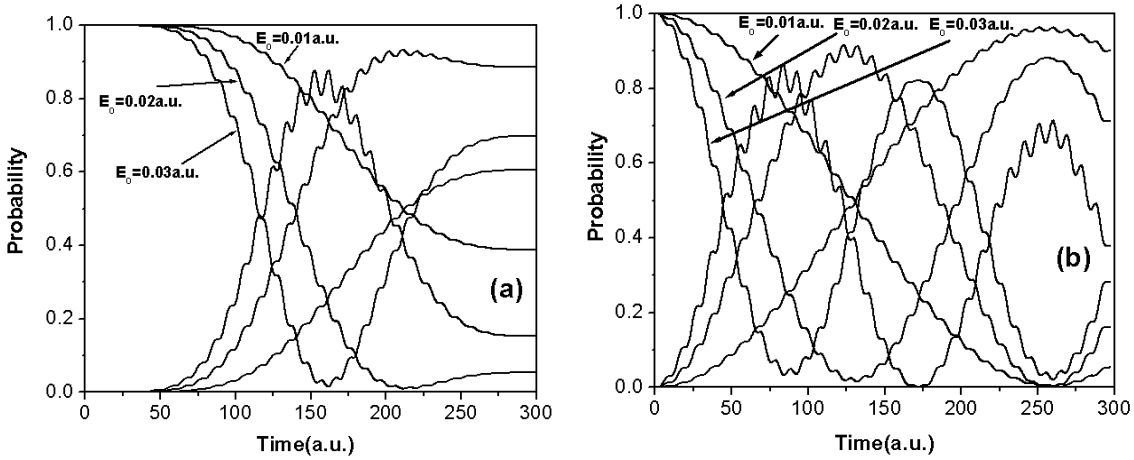

Figure 23: Rabi oscillation: (a) irradiated by the approximate Gauss pulse and (b) irradiated by the rectangular pulse.

wave function spreads outside both boundaries with the increasing of the laser intensity. The stronger the laser intensity is, the more widely the wave function spreads.

B. P-T Potential with Three Bound States

The P-T potential (5.12) for the parameters $U_0 = 0.7, \alpha_0 = 0.4$ possesses the three bound

DOI https://doi.org/2007-CiCP-7894 | Generated on 2024-12-22 17:59:56
OPEN ACCESS

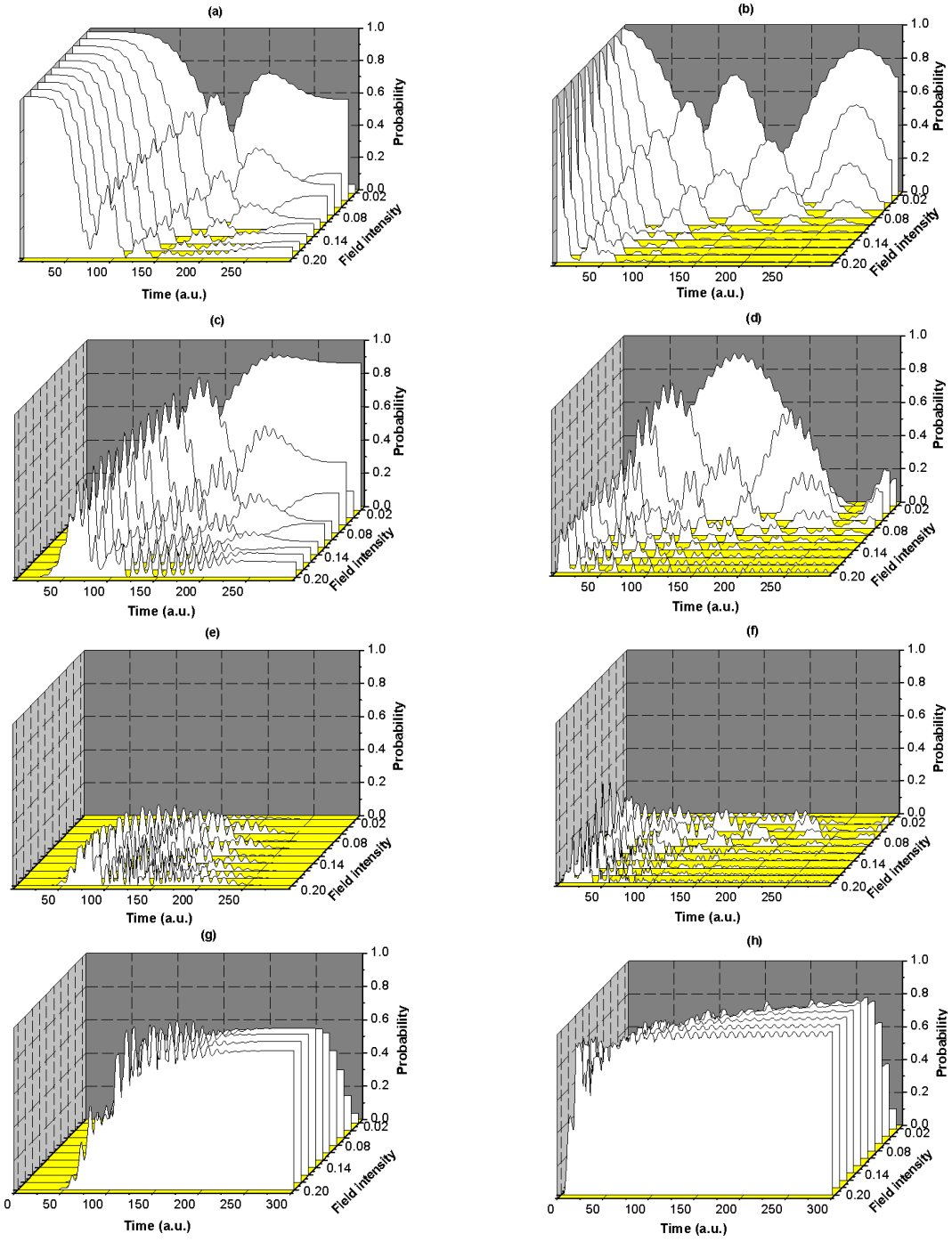

Figure 24: Population of the ground state, the first excited state, the second excited state and the ionization continuum in the laser field for the different laser pulse-shape: (a), (c), (e) and (g) irradiated by the approximate Gauss pulse, (b), (d), (f) and (h) irradiated by the rectangular pulse.

DOI https://doi.org/2007-CiCP-7894 | Generated on 2024-12-22 17:59:56
OPEN ACCESS

states, whose eigenenergies and corresponding normalized eigenfunctions are

$$E_0=-0.5a.u., \quad E_1=-0.18a.u., \quad E_2=-0.02a.u,$$
$$\varphi_0(x)=\frac{4}{\sqrt{15\pi}}(\cosh(\alpha_0 x))^{-2.5},$$
$$\varphi_1(x)=\frac{4}{\sqrt{5\pi}}(\cosh(\alpha_0 x))^{-1.5}\tanh(\alpha_0 x),$$
$$\varphi_2(x)=\sqrt{\frac{6}{5\pi}}\left[(\cosh(\alpha_0 x))^{-0.5}-\frac{4}{3}(\cosh(\alpha_0 x))^{-2.5}\right],$$

respectively. The ionization behaviors of the P-T potential are computed in the laser fields

$$\varepsilon(t)=\begin{cases}\varepsilon_0\sin(\omega_0 t) & (t_{on}\le t\le NT_0),\\ 0 & (NT_0\le t\le t_{off}),\end{cases}$$

and

$$\varepsilon(t)=\begin{cases}\varepsilon_0\sin^2(\omega_0 t/2N)\sin(\omega_0 t) & (t_{on}\le t\le NT_0),\\ 0 & (NT_0\le t\le t_{off}),\end{cases}$$

respectively, where $T_0=2\pi/\omega_0$ is the optical period of the laser field. In the following calculation, 15 optical periods are chosen as the pulse width, the ground state $\varphi_0(x)$ of the P-T potential as the initial input, and the laser frequency is chosen as the Rabi oscillation frequency between the ground state and the first excited state, which is $\omega_0=0.32a.u.$.

`(1): Rabi oscillation between the ground state and the first excited state.` When the laser intensity is weaker, the Rabi oscillation between the ground state and the first excited state will be the dominant process, and the transition rate between these energy levels will speed with the increase of the laser intensity, as shown in Fig. 23. This result is identical to that of the perturbation theory in traditional quantum mechanics. The oscillation depends strongly on the pulse-shape, and is suppressed faster for the rectangular pulse-shape than for the approximate Gauss pulse-shape with the increase of the laser intensity.

`(2): Population probability of each state for different pulse-shapes.` With the increase of the laser intensity, the effect of Rabi oscillation is weakened gradually and the ionization is strengthened; hence, the electron reaches directly the ionized continuum state by multi-photon ionization or tunneling ionization as well as over-barrier ionization. The population probability of the bound states

$$P_i(t)=|<\varphi_i(x)|\psi(x,t)>|^2$$

changes with the laser intensity for both the rectangular pulse-shape and the approximate Gauss pulse-shape, as shown in Fig. 24, which illustrates that the population probability of the bound states depends obviously on the pulse-shape. The probability of the electron recombination is greater for the approximate Gauss pulse-shape than the rectangular pulse-shape, and the population of the bound electron is greater for the approximate

DOI https://doi.org/2007-CiCP-7894 | Generated on 2024-12-22 17:59:56
OPEN ACCESS

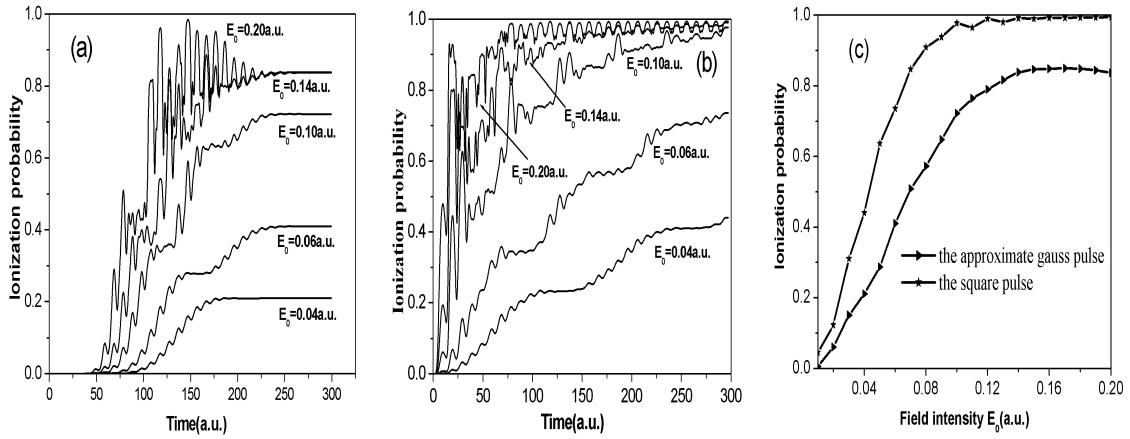

(a) (b) (c)

Figure 25: The ionization probability in the laser field: (a) irradiated by the approximate Gauss pulse, (b) irradiated by the rectangular pulse; and (c) for the two pulse-shapes.

Gauss pulse-shape than the rectangular pulse at the end of the laser pulse-shape at the time after the pulse.

The population probability of the continuum state is

$$P_c(t) = 1 - \sum_i P_i(t),$$

where the summation is over all the bound states and the result is also exhibited in Fig. 24. From this figure we can see that the ionization is strengthened with increasing laser intensity. In particular when the laser intensity reaches the critical intensity of $0.0625 a.u.$, the electron can freely go through the potential barrier and be ionized, which is called over-barrier ionization. When the laser intensity is greater than this value, the population of the continuum will be greater than that of the bound states, and thus the ionization will be the dominant process.

`(3): Ionization probability for different pulse-shapes.` The ionization probability is

$$P_{ion}(t) = 1 - \sum_i^n P_i(t) = 1 - \sum_i^n |<\varphi_i(x)|\psi(x,t)>|^2.$$

Fig. 25 shows that the ionization probability changes with time and the laser intensity for the two different pulse-shapes, Fig. 25(a) the approximate Gauss pulse-shape and Fig. 25(b) the rectangular pulse-shape. Fig. 25(c) is the curve of the ionization probability in the laser field at the time after the pulse. The figures illustrate that the ionization probability depends on the laser pulse-shape, but the total ionization trend is similar and the ionization amplitude is different for different pulse-shapes.

`(4): Probability density of the ionization continuum state with the laser`

DOI https://doi.org/2007-CiCP-7894 | Generated on 2024-12-22 17:59:56
OPEN ACCESS

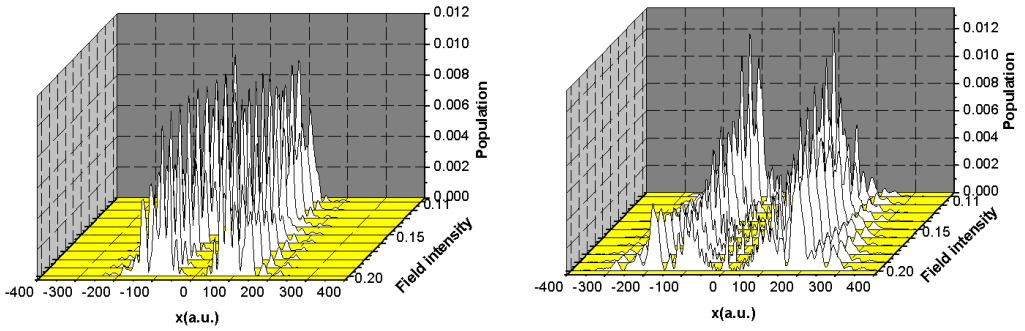

Figure 26: The ionization probability in the laser field: (a) irradiated by the approximate Gauss pulse, (b) irradiated by the rectangular pulse.

`intensity`. The probability density of the continuum state is

$$\rho_c = |\psi_c^*(x,t)\psi_c(x,t)|,$$

where $\psi_c(x,t) = \psi(x,t) - \sum_i <\varphi_i(x)|\psi(x,t)>\varphi_i(x)$ is the wave function of the ionized continuum state and the summation is over all the bound states. The curve of the probability density of the ionized continuum state in the laser field is displayed in Fig. 26; it illustrates that the spread of the electron is enhanced with the increase of the laser intensity in the space. The electron spreads more widely for the rectangular pulse-shape than the approximate Gauss pulse-shape.

The ionization and the recombination of the electron induced by the laser field depend obviously on the laser pulse-shape, which is the reason why the different pulse-shapes are adopted for the different physical problems. The rectangular pulse is adopted for the research on the ionization, because the electrons are ionized more for the rectangular pulse than the approximate Gauss pulse. However, the approximate Gauss pulse is adopted for the research on the high harmonic generation, because the high harmonic generation needs the electronic recombination process and the recombination probability is greater more for the approximate Gauss pulse than the rectangular pulse.

6 Conclusions

The symplectic methods are difference methods that preserve the symplectic structure. In this article, we have reviewed the applications of the symplectic methods for the classical Hamiltonian systems in quantum systems. Below we briefly summarize the main points of this work.

- Symplectic schemes for solving Hamiltonian systems are illustrated; explicit symplectic schemes for linear separate Hamiltonian systems and tailored to time-depend-

DOI https://doi.org/2007-CiCP-7894 | Generated on 2024-12-22 17:59:56
OPEN ACCESS

ent Hamiltonian functions, the Euler-centered scheme and symplectic Runge-Kutta scheme for a general Hamiltonian system are given.

- The classical theory and classical trajectory method is illustrated. The classical trajectories of a model molecule A_2B and diatomic system is calculated by means of symplectic and Runge-Kutta methods; the computation of quasiclassical trajectories for the $N(^4S)+O_2(X^3\Sigma_g^-)\rightarrow NO(X^2\Pi)+O(^3P)$ atmospheric reaction system is presented by means of both symplectic and Runge-Kutta methods. Comparisons are given. We show that symplectic methods are better methods in the calculation of classical trajectories of molecular systems. The classical dynamics of a molecular system in an intense laser field are studied by means of symplectic; the time-evolution of survival, dissociation, ionization and Coulomb explosion probability of H_2^+ in an intense laser field is analyzed.
- The symplectic schemes are extended to the numerical solution of the time-independent Schrödinger equation. We first transform the Schrödinger equation into a Hamiltonian canonical equation by using the Legendre transformation, and then introduce the symplectic scheme-shooting method (SSSM) to obtain the eigenvalues of the time-independent Schrödinger equation. Numerical methods based on the Magnus expansion and computations of the continuum eigenfunctions of the Schrödinger equation are also discussed.
- Asymptotic boundary conditions for solving the time-dependent Schrödinger equation of an atom in an intense laser field are given; symplectic discretizations based on the asymptotic boundary condition and the numerical eigenfunction expansion are implemented; and the multi-photon ionization, above-threshold ionization, Rabbi oscillation and high-order harmonic generation of laser-atom interaction are discussed.

Acknowledgments

This research was supported in part by the National Natural Science Foundation of China (#10574057, #10571074, and #10171039), and by the Specialized Research Fund for the Doctoral Program of Higher Education (#20050183010). The other members of our research group include Shi-xing Liu, Yu-hua Chi, Wei Hua, Jia-yu Wei, and Chun-li Zhang.

References

[1] H. Goldstein, Classical Mechanics, Addison-Wesley, Reading, Massachusetts, 1950.
[2] V. I. Arnold, Mathematical Method of Classical Mechanics, Springer, Verlag, 1978.
[3] R. D. Ruth, A Canonical integration technique, IEEE T. Nucl. Sci., NS-30 (1983), 2669-2671.
[4] K. Feng (Ed.), Proc. of the 1984 Beijing Symposium on Differential Geometry and Differential Equations. Computation of Partial Differential Equations, Science Press, Beijing, 1985, pp. 42-58.
[5] K. Feng, Difference schemes for Hamiltonian formalism and symplectic geometry, J. Comput. Math., 4(3) (1986), 279-289.

DOI https://doi.org/2007-CiCP-7894 | Generated on 2024-12-22 17:59:56
OPEN ACCESS

[6] K. Feng, H. M. Wu, M. Z. Qin and D. L. Wang, Construction of canonical difference schemes for Hamiltonian formalism via generating functions, J. Comput. Math., 7(1) (1989), 71-96.
[7] H. Yoshida, Construction of higher order symplectic integrators, Phys. Lett. A, 150 (1990), 262-268.
[8] M. Z. Qin and M. Q. Zhang, Multi-stage symplectic schemes of two kind of Hamiltonian system of wave equations, Comput. Math. Appl., 19(10) (1990), 51-62.
[9] J. E. Marsden and T. S. Ratiu, Introduction to Mechanics and Symmetry, Springer, Verlag, 1997.
[10] G. Sun, Symplectic partitioned Runge-Kutta methods, J. Comput. Math., 11 (1993), 365.
[11] J. M. Sanz-Serna and M. P. Calvo, Numerical Hamiltonian Problems, Chapman and Hall, London, 1994.
[12] Y. B. Suris, Partitioned Runge-Kutta methods as phase volume-preserving integrators, Phys. Lett. A, 220 (1996), 63-69.
[13] J. L. Hong and Y. Liu, Symplectic integrations of linear discontinuous Hamiltonian systems and an application to the numerical simulation of bounded solutions, Neural Parallel Sci. Comput., 8 (2000), 317-325.
[14] Z. J. Shang, Resonant and diophantine step sizes in computing invariant tori of Hamiltonian systems, Nonlinearity, 13 (2000), 299-308.
[15] P. J. Channell and J. C. Scovel, Symplectic integration of Hamiltonian system, Nonlinearity, 3 (1990), 213-259.
[16] H. Yoshida, Recent progress in the theory and application of symplectic integrators, Celest. Mech. Dyn. Astr., 56 (1993), 27-43.
[17] M. Suzuki, General theory of higher-order decomposition of exponential operators and symplectic integrators, Phys. Lett. A, 165 (1992), 387-395.
[18] E. Forest and R. D. Ruth, Fourth-order symplectic integration, Physica D, 43 (1990), 105-117.
[19] E. Hairer, Variable time step integration with symplectic methods, Appl. Numer. Math., 25 (1997), 219-227.
[20] G. R. W. Quispel and H. W. Capel, Solving ODEs numerically while preserving a first integral, Phys. Lett. A, 218 (1996), 223-228.
[21] S. Reich, Momentum conserving symplectic integrators, Physica D, 76 (1994), 375.
[22] J. M. Sanz-Serna and A. Portillo, Classical numerical integrators for wave-packet dynamics, J. Chem. Phys., 104(6) (1996), 2349-2355.
[23] S. A. Chin, and C. R. Chen, Fourth order gradient symplectic integrator methods for solving the time-dependent Schrödinger equation, J. Chem. Phys., 114 (2001), 7338-7341.
[24] P. F. Zhao and M. Z. Qin, Multi-symplectic geometry and multi-symplectic Preissmann scheme for the KdV equation, J. Phys. A-Math. Gen., 33 (2000), 3613-3626.
[25] S. Reich, Multi-symplectic Runge-Kutta collocation methods for Hamiltonian wave equations, J. Comput. Phys., 157 (2000), 473-499.
[26] J. Marsden and S. M. Shkollor, Multi-symplectic geometry, covariant Hamiltonians and water waves, Math. Proc. Camb. Phil. Soc, 125 (1999), 553-575.
[27] T. J. Bridge, Multi-symplectic structure and wave propagation, Math. Proc. Camb. Phil. Soc., 121 (1997), 147-190.
[28] Y. F. Tang, L. Vázquez, F. Zhang and V. M. P'erez-García, Symplectic methods for the nonlinear Schrödinger equation, Comput. Math. Appl., 32(5) (1996), 73-83.
[29] X. S. Liu and P. Z. Ding, Dynamic properties of cubic nonlinear Schrödinger equation with varying nonlinear parameters, J. Phys. A, 37 (2004), 1589-1602.
[30] X. S. Liu and P. Z. Ding, Behaviour of cubic nonlinear Schrödinger equation by using the

DOI https://doi.org/2007-CiCP-7894 | Generated on 2024-12-22 17:59:56
OPEN ACCESS

symplectic method, Chinese Phys. Lett., 21(2) (2004), 230-232.
[31] X. S. Liu, J. Y. Wei and P. Z. Ding, Dynamic properties of the cubic nonlinear Schrödinger equation by symplectic method, Chinese Phys., 14(2) (2005), 231-237.
[32] J. L. Hong and Y. Liu, A novel numerical approach to simulating nonlinear Schrödinger equation with varying coefficients, Appl. Math. Lett., 16 (2003), 759-765.
[33] X. H. Liao and L. Liu, Applications of symplectic algorithms to the numerical researches of restricted three-body problem, Chinese J. Comput. Phys., 12(1) (1995), 102-108.
[34] Y. Zhao, B. Wang and Z. Z. Ji, Symplectic-like difference schemes for generalized Hamilton system, Adv. Atmos. Sci., 19 (2002), 719-726.
[35] B. Gladman, M. Duncan and J. Candy, Symplectic integrators for long-term integrations in celestial mechanics, Celest. Mech. Dyn. Astr., 52 (1991), 221-240.
[36] W. S. Zhu, X. S. Zhao and Y. Q. Tang, New time-dependent methods in quantum scattering, J. Chem. Phys., 104(6) (1996), 2271-2274.
[37] W. S. Zhu, X. S. Zhao and Y. Q. Tang, Numerical methods with a high order of accuracy applied in the quantum system, J. Chem. Phys., 104(6) (1996), 2275-2286.
[38] S. K. Gray and J. M. Verosky, Classical Hamiltonian structures in wave packet dynamics, J. Chem. Phys., 100(7) (1994), 5011-5022.
[39] S. K. Gray and D. E. Manolopoulos, Symplectic integrators tailored to the time-dependent Schrödinger equation, J. Chem. Phys., 104(18) (1996), 7099-7112.
[40] S. D. Bond, B. J. Leimkuhler and B. B. Laird, The Nosé-Poincaré method for constant temperature molecular dynamics, J. Comput. Phys., 151(1) (1999), 114-134.
[41] J. B. Sturgeon and B. B. Laird, Symplectic algorithm for constant-pressure molecular dynamic Using a Nosé-Poincaré Thermostat, J. Chem. Phys., 12(8) (2000), 3474-3482.
[42] J. R. Cary and I. Doxas, An explicit symplectic integration scheme for plasma simulations, J. Comput. Phys., 107 (1993), 98-104.
[43] P. Z. Ding, C. X. Wu, Y. K. Mu, Y. X. Li and M. X. Jin, Square-preserving and symplectic structure and scheme for quantum system, Chinese Phys. Lett., 13(4) (1996), 245-248.
[44] X. S. Liu and P. Z. Ding, New progress of structure-preserving computation for quantum system, Prog. Phys., 24(1) (2004), 48-91, in Chinese.
[45] A. Banerjee and N. P. Adams, Separation of classical equation of motion based on symmetry, J. Chem. Phys., 91(9) (1989), 5444-5450.
[46] Y. X. Li, P. Z. Ding, M. X. Jin and C. X. Wu, Computing classical trajectories of model molecule AB by symplectic algorithm, Chem. J. Chinese Univ., 15(8) (1994), 1181-1186, in Chinese.
[47] J. F. He, W. Hua, X. S. Liu and P. Z. Ding, Computation of quasiclassical trajectories by symplectic algorithm for the $N(^4S)+O_2(X^3\sum_g^-)\rightarrow NO(X^2\Pi)+O(^3P)$ reaction system, J. Math. Chem., 37 (2005), 127-138.
[48] J. F. He, S. X. Liu, X. S. Liu and P. Z. Ding, A quasiclassical trajectory study for the $N(^4S)+O_2(X^3\sum_g^-)\rightarrow NO(X^2\Pi)+O(^3P)$ atmospheric reaction based on a new ground potential energy surface, Chem. Phys., 315 (2005), 87-96.
[49] P. Warneck, Chemistry of The Natural Atmosphere, Academic Press, San Diego, 1998, Chapter 3.
[50] N. Balakrishnam, E. Sergueeva, V. Kharchenko and A. Dalgarno, Kinetics and thermalization of hot $N(^4S)$ atoms in the upper atmosphere, J. Geophys. Res., 105 (2000), 18549-18556.
[51] R. Sayós, C. Oliva and M. González, New analytical ($^2A'$,$^4A'$) surfaces and theoretical rate constants for the $N(^4S)+O_2$ reaction, J. Chem. Phys., 117 (2002), 670-679.
[52] M. Gilibert, A. Aguilar, M. González and R. Sayós, A quasiclassical trajectory study of

DOI https://doi.org/2007-CiCP-7894 | Generated on 2024-12-22 17:59:56
OPEN ACCESS

the effect of the initial rovibrational level and relative translational energy of reactants on the dynamics of the $N(^4S_u)+O_2(X^3\sum_g^-)\rightarrow NO(X^2\Pi)+O(^3P_g)$ atmospheric reaction on the $^2A'$ ground potential energy surface, Chem. Phys., 178 (1993), 287-303.

[53] R. Sayós, A. Aguilar, M. Gilibert and M. González, Orientational dependence of the $N(^4S)+NO(X^2\Pi)$ and $N(^4S)+O_2(X^3\sum_g^-)$ reactions: Comparison of the angle-dependent line-of-centers model with quasiclassical trajectories, J. Chem. Soc. Faraday Trans., 89 (1993), 3223-3234

[54] J. T. Lin, T. L. Lai, D. S. Chuu and T. F. Jiang, Quantum dynamics of a diatomic molecule under chirped laser pulses, J. Phys. B, 31 (1998), L117-L126.

[55] J. T. Lin and T .F. Jiang, Cantori barriers in the excitation of a diatomic molecule by chirped pulses, J. Phys. B, 32 (1999), 4001-4012.

[56] Y. Gu and J. M. Yuan, Classical dynamics and resonance structures in laser-induced dissociation of a Morse oscillator, Phys. Rev. A, 36 (1987), 3788-3795.

[57] W. Qu, S. Hu and Z. Xu, Classical dynamics of H_2^+ interacting with an ultrashort intense laser pulse, Phys. Rev. A, 57 (1998), 2219-2222.

[58] Y. W. Duan, W. K. Liu and J. M. Yuan, Classical dynamics of ionization, dissociation, and harmonic generation of a hydrogen molecular ion in intense laser fields: A collinear model, Phys. Rev. A, 61 (2000), 053403.

[59] S. Chelkowski, C. Foisy and A. D. Bandrauk, Electron-nuclear dynamics of multiphoton H_2^+ dissociative ionization in intense laser fields, Phys. Rev. A, 57 (1998), 1176-1185.

[60] X. S. Liu, X. Y. Liu, Z. Y. Zhou, P. Z. Ding and S. F. Pan, Numerical solution of one-dimensional time-independent Schrödinger equation by using symplectic schemes, Int. J. Quantum Chem., 79(6) (2000), 343-349.

[61] X. S. Liu, L. W. Su and P. Z. Ding, Symplectic algorithm for use in computing the time-independent Schrödinger equation, Int. J. Quantum Chem., 87(1) (2002), 1-11.

[62] X. S. Liu, Y. H. Chi and P. Z. Ding, Symplectic schemes and the shooting method for eigenvalues of the Schrödinger equation, Chinese Phys. Lett., 21(9) (2004), 1681-1684.

[63] S. F.-P. Paul and H. Fouckhardt, An improved shooting approach for solving the time-independent Schrödinger equation for III/V QW structures, Phys. Lett. A, 286 (2001), 199-204.

[64] F. Zho, Z. Cao and Q. Shen, Energy splitting in symmetric double-well potentials, Phys. Rev. A, 67 (2003), 062112.

[65] H. Hairer, C. Lubich and G. Wanner, Geometric Numerical Integration, Springer Series in Computational Mathematics 31, Springer-Verlag, Berlin, New York, 2002, Chapter 4.

[66] X. S. Liu and P. Z. Ding, Numerical method based on the Magnus expansion and a new shooting method for eigenvalues of Schrödinger equation, Int. J. Quantum Chem., 103(2) (2005), 149-156.

[67] X. S. Liu, X. Y. Liu and P. Z. Ding, Symplectic scheme in the calculation of 1-dimensional model of strong field, Chinese Science Abstracts, 6(8) (2000), 994-995.

[68] X. S. Liu, X. Y. Liu, Y. J. Yang, P. Z. Ding and Q. R. Zhu, Wronskian-preserving algorithm of one-dimensional model in the strong laser field, Chinese J. Comput. Phys., 18(6) (2001), 487-490.

[69] Y. Y. Qi, X. S. Liu and P. Z. Ding, Continuum eigen-functions of 1-D time-independent Schrödinger equation solved by symplectic algorithm, Int. J. Quantum Chem., 101(1) (2005), 21-26.

[70] X. S. Liu, L. W. Su, X. Y. Liu and P. Z. Ding, Numerical solution of a two-dimensional time-independent Schrödinger equation by using symplectic schemes, Int. J. Quantum Chem.,

DOI https://doi.org/2007-CiCP-7894 | Generated on 2024-12-22 17:59:56
OPEN ACCESS

83(5) (2001), 303-309.
[71] G. Psihoyios and T. E. Simos, Effective numerical approximation of Schrödinger type equations through multiderivative exponentially-fitted schemes, Appl. Num. Anal. Comp. Math., 1(1) (2004), 205-215.
[72] Z. Kalogiratou, Th. Monovasilis and T. E. Simos, Symplectic integrators for the numerical solution of the Schrödinger equation, J. Comput. Appl. Math., 158 (2003), 83-92.
[73] K. Tselios and T. E. Simos, Symplectic methods of fifth order for the numerical solution of the radial Schrödinger equation, J. Math. Chem., 35 (2004), 55-63.
[74] T. E. Simos and J. Vigo-Aguiar, On the construction of efficient method for second order IVPS with oscillating solution, Int. J. Mod. Phys. C, 12(10) (2001), 1453-1476.
[75] T. E. Simos, Multiderivative method for the numerical solution of Schrödinger equation, MATCH: Commun. Math. Comput. Chem., 50 (2004), 7-26.
[76] Th. Monovasilis and T. E. Simos, Numerical solution of the two-dimensional time independent Schrödinger equation by third order symplectic schemes, Chem. Phys., 313 (2005), 293-298
[77] X. X. Zhou and C. D. Lin, Linear-least-squares fitting method for the solution of the time-dependent Schrödinger equation: Applications to atoms in intense laser fields, Phys. Rev. A, 61 (2000), 053411.
[78] D. G. Lappas and A. L'Huillier, Generation of attosecond xuv pulses in strong laser-atom interactions, Phys. Rev. A, 58 (1998), 4140-4146.
[79] M. Schnürer, Ch. Spielmann, P. Wobrauschek, C. Streli, N. H. Burnett, C. Kan, K. Ferencz, R. Koppitsch, Z. Cheng, T. Brabec and F. Krausz, Coherent 0.5-keV x-ray emission from helium driven by a sub-10-fs laser, Phys. Rev. Lett., 80 (1998), 3236-3239.
[80] X. S. Liu, Y. Y. Qi, W. Hua and P. Z. Ding, Behaviors and high-order harmonic generation for short-range model potential in the intense laser field by using the symplectic algorithm, Prog. Nat, Sci., 14(7) (2004), 573-581.
[81] X. Y. Liu, X. S. Liu, P. Z. Ding and Z. Y. Zhou, The symplectic algorithm for use in a model of laser field, in: J. J. Rocca, et al. (Eds), X-Ray Lasers 2002: 8th International Conference on X-Ray Lasers, AIP Conference Proceedings, 641(1) (2002), 265-270.
[82] J. Heading, An Introduction to Phase Integral Methods, Methuen and Co., London, 1962.
[83] R. D. Cowan, The Theory of Atomic Structure and Spectra, University of California Press, Berkeley, 1981, p. 535.
[84] A. M. Ermolaev, I. V. Puzynin, A. V. Selin and S. I. Vinitsky, Integral boundary conditions for the time-dependent Schrödinger equation: Atom in a laser field, Phys. Rev. A, 60 (1999), 4831-4845.
[85] K. Boucke, H. Schmitz and H.-J. Kull, Radiation conditions for the time-dependent Schrödinger equation: Application to strong-field photoionization, Phys. Rev. A, 56 (1997), 763-771.
[86] Y.-J. Sun and M. Z. Qin, A multi-symplectic scheme for RLW equation, J. Comput. Math., 22 (2004), 611-621.

DOI https://doi.org/2007-CiCP-7894 | Generated on 2024-12-22 17:59:56
OPEN ACCESS